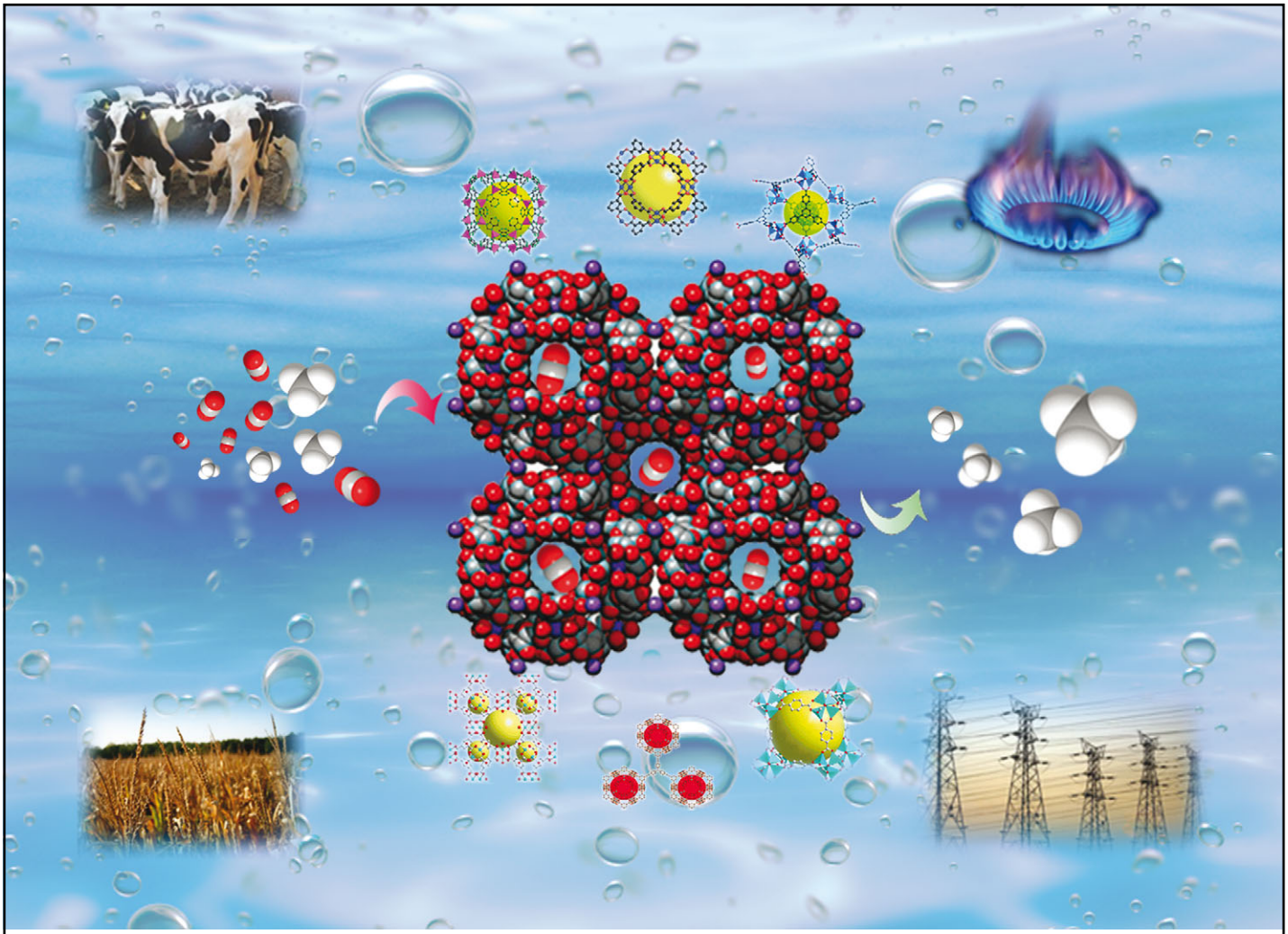

Featuring research from the group of Professor Francis Verpoort at Laboratory of Organometallics, Catalysis and Ordered Materials, State Key Laboratory of Advanced Technology for Materials Synthesis and Processing, Wuhan University of Technology, Wuhan, P.R. China.

Metal–organic frameworks for upgrading biogas *via* CO_2 adsorption to biogas green energy

The upgrading abilities of biogas employing metal–organic frameworks (MOFs) at atmospheric conditions hold many challenges. This review discusses the key factors to improve MOF materials for high CO_2 capture and selectivity to produce bio-methane and to reduce the fossil fuel CO_2 emission.

As featured in:

See Somboon Chaemchuen *et al.*, *Chem. Soc. Rev.*, 2013, **42**, 9304.

RSC Publishing

www.rsc.org/chemsocrev

Registered Charity Number 207890

Chem Soc Rev

RSC Publishing

REVIEW ARTICLE

View Article Online
View Journal | View Issue

Cite this: *Chem. Soc. Rev.*, 2013, **42**, 9304

Metal–organic frameworks for upgrading biogas *via* CO_2 adsorption to biogas green energy

Somboon Chaemchuen,[ab] Nawsad Alam Kabir,[ab] Kui Zhou[ab] and Francis Verpoort*[abcd]

Received 9th July 2013

DOI: 10.1039/c3cs60244c

www.rsc.org/csr

In the midst of the global climate change phenomenon, mainly caused by fossil fuel burning to provide energy for our daily life and discharge of CO_2 into the atmosphere, biogas is one of the important renewable energy sources that can be upgraded and applied as a fuel source for energy in daily life. The advantages of the production of hybrid materials, metal–organic framework (MOF) adsorbents, expected for the biogas upgrading, rely on the bulk separation of CO_2 under near-ambient conditions. This review highlights the challenges for MOF adsorbents, which have the greatest upgrading abilities for biogas *via* selective passage of methane. The key factors improving the ideal MOF materials for these high CO_2 capture and selectivity uses for biogas upgrading to produce bio-methane and reduce fossil-fuel CO_2 emission will be discussed.

1. Introduction

Fossil fuels have been used in prodigious amounts to power human society over the past 200 years and even currently, over 85% of the global energy demand is met by fossil fuel burning.[1] The reasons for this skewed reliance on fossil fuels as our primary energy source are due to the inherent energy density, abundance, and the economic dependence of modern society on the acquisition and trade of these resources. The rapid increase of the energy demand due to the increase of global

[a] *Laboratory of Organometallics, Catalysis and Ordered Materials, State Key Laboratory of Advanced Technology for Materials Synthesis and Processing, Wuhan University of Technology, Wuhan, China. E-mail: francis.verpoort@ugent.be; Fax: +86-27-87879468; Tel: +86-27-87665259*

[b] *Center for Chemical and Material Engineering, Wuhan University of Technology, Wuhan 430070, P.R. China*

[c] *Department of Applied Chemistry, Faculty of Sciences, Wuhan University of Technology, Wuhan 430070, P.R. China*

[d] *Department of Inorganic and Physical Chemistry, Laboratory of Organometallic Chemistry and Catalysis, Ghent University, 9000 Ghent, Belgium*

Somboon Chaemchuen

Somboon Chaemchuen (1984, Thailand) received his PhD in Chemical Engineering from Chulalongkorn University, Thailand, in 2011 under the supervision of Dr Suphot Phatanasri. In 2010, he went to Aachen University, Germany, for research collaboration with Prof. Wolfgang F. Holderich. He has recently obtained a postdoctoral position in the group of Prof. Francis Verpoort at the State Key Laboratory of Advanced Technology for Materials Synthesis and Processing, Wuhan University of Technology. His current research interests are the preparation of metal–organic framework (MOF) compounds and the study of their applications.

Nawsad Alam Kabir

Nawsad Alam Kabir (1980, Bangladesh) received his MSc in Chemical Engineering & Management degree from the University of Glasgow, Scotland, in 2011. He is currently a PhD candidate under the supervision of Prof. Francis Verpoort from the Laboratory of Organometallics, Catalysis and Ordered Materials, State Key Laboratory of Advanced Technology for Materials Synthesis and Processing, Wuhan University of Technology. His current research interests are focused on the design and synthesis of metal–organic frameworks (MOFs).

population and the industrialization of more and more countries have led to drastic changes in the composition of the Earth's atmosphere. Carbon dioxide is the main by-product of the combustion of fossil fuel, besides, it is one of the main compounds of greenhouse gases (GHG). It is reported that combustion accounts for 86% of anthropogenic greenhouse gas emission, with the remainder arising from land use changes (primarily deforestation) and chemical processing.[2] Modern climate science predicts that the accumulation of greenhouse gases in the atmosphere will contribute to an increase in surface air temperature of 5.2 °C between the years 1861 and 2100.[3] A critical point solution of a multifaceted problem requires shared vision and worldwide collaborative efforts from governments, policy makers and economists, as well as scientists, engineers and venture capitalists. This must be complemented by crucial strategies such as improving energy, switching to less carbon-intensive fuel (*i.e.* natural gas), and phasing in the use of renewable energy resources such as solar, wind, biomass, *etc.*

Biogas is a very interesting source of renewable energy, with methane (CH_4) as the main component. Biogas can be upgraded to produce high quality fuel (bio-methane) for use as an alternative fuel in the immediate future. In view of environmental regulations, methane is the most important non-CO_2 greenhouse gas (GHG), accounting for 10% of total GHG emissions in developed countries and almost 20% in developing countries.[4] The greenhouse warming potential (GWP) of methane is 21 times higher and the lifetime of methane molecules in the atmosphere is 10 times longer than carbon dioxide molecules. Furthermore, any reduction of methane emission in the atmosphere is much more important in the short- and medium-term. Meanwhile, it can reduce the associated greenhouse gas emissions in line with global targets. The demand for biogas is expected to increase continuously in the coming years, because of its ability to produce lower CO_2 emissions than other fossil fuels as shown in Fig. 1.[5] In several countries, there is a specific legislation with regard to the use of renewable energy for production of fuels in order to promote this industry. Actually, several countries (United States, Sweden, France, Germany, Denmark, The Netherlands, *etc.*) produce fuel grade methane from biogas.

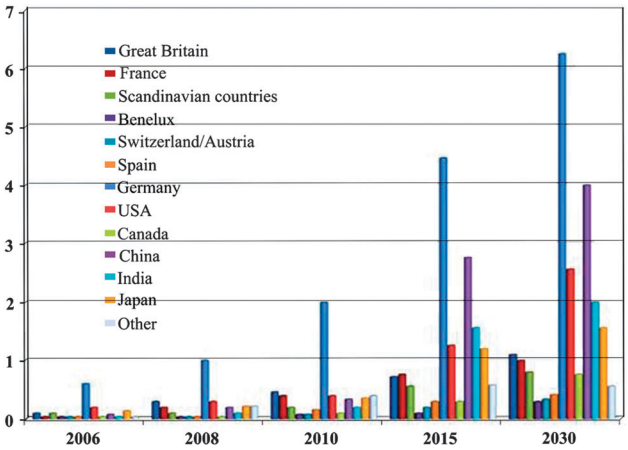

Fig. 1 Market of biogas plants worldwide in 2006–2030 by leading countries, in US$ billion (Source: Helmut Kaiser Consultancy).[5]

1.1 General background of biogas

Biogas typically refers to a gas produced by breakdown of organic matter in the absence of oxygen. Organic waste material such as

Kui Zhou

Kui Zhou (1990, China) received his bachelor degree in Material Science & Technology (Wuhan University of Technology, China) in 2012. He is currently a master student under the supervision of Prof. Francis Verpoort from the Laboratory of Organometallics, Catalysis and Ordered Materials (LOCOM), State Key Laboratory of Advanced Technology for Materials Synthesis and Processing, Wuhan University of Technology. His current research interests are in synthesis and modification of metal–organic frameworks (MOFs).

Francis Verpoort

Francis Verpoort (1963, Belgium) received his DPhil from Ghent University in 1996. In 1998, he became a full professor at the same university. In 2004, he founded a spin-off company of Ghent University based on (latent) ruthenium olefin metathesis catalysts. In 2008, he became an Editor of Applied Organometallic Chemistry. Currently, next to Full Professor at Ghent University, he is a chair professor at the State Key Laboratory of Advanced Technology for Material Synthesis and Processing (Wuhan University of Technology) and Director of the Center for Chemical and Material Engineering (Wuhan University of Technology). Recently, he has been appointed as "Expert of the State" in the frame of "Thousand Talents" program, PR China. His main research interests concern the structure and mechanisms in organometallic material chemistry, homogeneous and heterogeneous catalysts, MOFs, water splitting, olefin metathesis and its applications, CO_2 conversion, and inorganic and organic polymers.

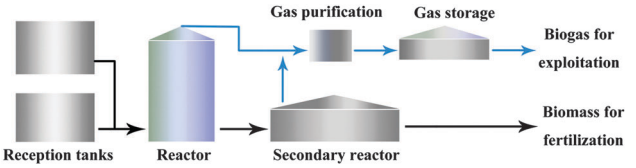

Fig. 2 Schematic diagram of a biogas plant.

dead plants and animals, animal faeces, and kitchen waste can be converted into a gaseous fuel called biogas. Biogas is produced by the anaerobic digestion or fermentation of biodegradable materials.[6] Biogas originates from biogenic material and is a type of biofuel. The process steps of biogas production are depicted in Fig. 2. Biogas comprises primarily methane (CH_4) and carbon dioxide (CO_2) and may have small amounts of hydrogen sulphide (H_2S), moisture and siloxanes. The different substances have an impact on the methane yield as shows in Table 1.[7] The amount of these contaminants strongly depends on the source of the biogas. These gases may be removed sequentially,[8] starting with sulphur compounds and then water.[9] Finally, the mixture of CO_2 and CH_4 must be separated. Methane is the smallest hydrocarbon molecule with a low heating value of 50 MJ kg^{-1} (35.7 MJ Nm^{-3}). When compared with other carbon-based fuels, methane presents a lower emission factor: 57.3 tons of CO_2 per TJ of energy. A low emission factor combined with the renewable origin of the fuel is beneficial from many points of view. The separation of CO_2 from methane is essential for the upgrading and the treatment of biogas to improve purity and reduce pipeline corrosion induced by carbonic acid.[10] A more potentially promising scenario is that a considerable fraction of the captured CO_2 could be applied in its conversion into a fuel for transportation, provided that efficient methods for carrying out the conversion *via* a renewable energy source can be developed.[11,12]

1.2 Current technology for biogas upgrading

Indeed, biogas has been identified as a tropical area in green chemistry and green energy because of its implications for global warming and national economies. Carbon dioxide is the major biogas contaminant, and reduces the caloric content of biogas. A typical municipal or industrial biogas consists of approximately 30–40% CO_2, which is comparable with other gas sources given in Table 2. On the economic side, the removal of carbon dioxide is the most critical step in biogas upgrading. The upgrading of biogas (CO_2 removal) takes between 3–6% of the energy of biogas and may cost up to €10/GJ in small streams.[13]

Several approaches have been proposed to separate CO_2 from gas mixtures such as absorption, cryogenic distillation, membrane separation, and adsorption. Current technologies involving aqueous amine absorbents (liquid media) capturing CO_2 from the gas mixture with a high selectivity but at high cost primarily require a large energy input for regeneration of the captured material as shown in Fig. 3.[14] Here, the energy penalty originates primarily from the need to heat the large quantity of water in which the amine is dissolved, as well as the energy required to break the C–N bond that is formed during the interaction between CO_2 and the amine functionality. Cryogenic distillation, although widely used for the separation of other gases, is generally not considered as a practical means to separate CO_2 from flue gases because of the high-energy costs involved. Membranes have been extensively studied for CO_2 separation from relatively concentrated sources, such as natural gas deposits.[15] They can be highly efficient mass-separating agents, especially when the species that are to pass through the membrane are present at high concentration. Adsorption processes for gas separation *via* selective adsorption on solid media (adsorbent) are also well known.[16,17] Solid adsorbents are typically employed in cyclic, multi-module processes of adsorption and desorption, and the two main methods for configuring an adsorption process are pressure-swing adsorption (PSA)[18a] and temperature-swing adsorption (TSA).[18b] In a PSA process, the adsorbent is regenerated by lowering the pressure, whereas in a TSA process, the regeneration is carried out by increasing the temperature.[19] Although TSA is more effective in cleaning the adsorbent, it has the disadvantage of relatively slow heating and cooling steps. For this reason, TSA is limited to the removal of small quantities of strongly adsorbed impurities.[20] Because of the low energy requirement and fast regeneration,[21] PSA is now used as a commercial technology for a number of applications. If the regeneration pressure is less than 1 atm, the process is referred to as vacuum-swing adsorption (VSA).[22] For flue gas separation processes, VSA is considered to be more promising than regular PSA because pressurizing the large feed stream is cost prohibitive.[23] VSA seems to be an interesting process to extend to locations with small and medium flow rates and with mild temperatures, particularly to be employed within the Clean Development Mechanism of the Kyoto protocol. Tables 3 and 4 summarize technologies and their performances for biogas upgrading which are currently available and in operation.[13] Table 5 compares various biogas-upgrading

Table 1 Biogas and methane yield at complete digestion of biomass from different classes of substrates

Organic substance	Process	Gas yield, STP[a]		
		ml biogas/g	ml CH_4/g	% CH_4
Cellulose	$(C_6H_{10}O_5)_n + nH_2O \rightarrow 3nCH_4 + 3nCO_2$	830	415	50.0
Protein	$2C_5H_7NO_2 + 8H_2O \rightarrow 5CH_4 + 3CO_2 + 2(NH_4)(HCO_3)$	793	504	63.6
Fat[b]	$C_{57}H_{104}O_6 + 28H_2O \rightarrow 40CH_4 + 17CO_2$	1444	1014	70.2

[a] STP = standard temperature and pressure (0 °C and 1 atm). [b] Glycerol trioleic acid.

Table 2 Composition of biogas, landfill gas and natural gas

Compounds	Biogas	Landfill gas	Natural gas (Danish)[a]	Natural gas (Dutch)
Methane (vol%)	60–70	35–65	89	81
Other hydrocarbons (vol%)	0	0	9.4	3.5
Hydrogen (vol%)	0	0–3	0	—
Carbon dioxide (vol%)	30–40	15–50	0.67	1
Nitrogen (vol%)	~0.2	5–40	0.28	14
Oxygen (vol%)	0	0.5	0	0
Hydrogen sulphide (ppm)	0–4000	0–100	2.9	—
Ammonia (ppm)	~100	~5	0	—
Lower heating value (kWh Nm^{-3})	6.5	4.4	11.0	8.8

[a] Average during 2007 (http://www.Energinet.dk).

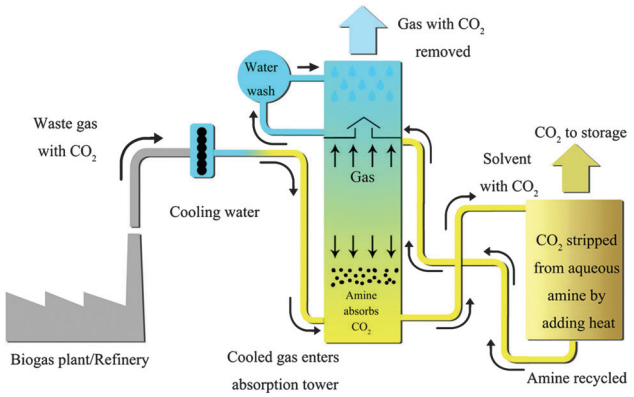

Fig. 3 Carbon dioxide capture plant by liquid amines (Source: TCM).[14]

processes in terms of process parameters and operation & cost efficiencies.[24]

An adsorbent for a fixed-bed adsorption process has been a key factor in the design of the operation unit for the purification and bulk separation of gas mixtures for PSA or VSA processes. All properties of the cycle (operating conditions and operating mode) depend on the initial choice of the adsorbent. The porous adsorbing materials have also been widely used for separating CO_2 from various sources. Various adsorbents have been considered for CO_2 separation and capture, including microporous and mesoporous materials (activated carbon, carbon molecular sieves, zeolites and chemically functionalized mesoporous materials), metal oxides, and so on.[25] Most studies of CO_2–CH_4 separation have focused on zeolites[26–30] and carbon-based adsorbents[30–34] of which the adsorption equilibrium isotherms for CO_2 and CH_4 are shown in Fig. 4 and 5 respectively.[35] Recently, metal–organic frameworks (MOFs) have been recognized as a new family of porous materials that have potential applications in separation, sensing, gas storage, and catalysis.[36–38] The synthetic strategy opens up the possibility to systematically vary pore size and chemical functionalities in the search for an optimal adsorbent. An additional advantage of using MOFs for separation is that they can be regenerated under milder conditions than most zeolites, which require considerable heating and the associated high costs.[39]

There are several commercial technologies to remove CO_2 from biogas streams. So far, of all technologies, there is no unique technology for upgrading since the behaviour of all technologies is quite similar and their capacities all decrease with increasing plant capacity. The selection of an appropriate technology to upgrade biogas depends on operation conditions, legislation, *etc.*

1.3 Removal of the main impurities from biogas

Hydrogen sulphide (H_2S) removal. H_2S is formed during microbiological reduction of sulphur containing compounds (sulphates, peptides, amino acids, *etc.*) in biogas processes. Hydrogen sulphide is a colourless, very poisonous, flammable gas with the characteristic odor of rotten eggs. The combination with water (present in biogas) creates sulphuric acid, which is a very corrosive acid, responsible for the corrosion of metallic parts like tanks and tubes, and brittle cracking of metals due to hydrogen, which can result in breaking of the tanks or piping. Although biogas has contributed to provide energy for daily life, burning H_2S in biogas will form sulphur dioxide, which causes environmental pollution. Therefore, the removal of H_2S is a critical issue, encouraged to protect the environment and the equipment. For enhancing the safety of technology systems there is a critical need for expanding research involving the removal of H_2S from biogas. For the removal of hydrogen sulphide from biogas several technologies have been developed such as precipitation in the digester liquid, adsorption on an adsorbent, chemical absorption and so on. An overview and description of the recent technologies to remove H_2S from biogas is given in Table 6.[40]

Table 3 General data of currently available technologies for upgrading biogas

Principle	Name	Type of regeneration	Pretreatment	Working pressure (bars)	Methane losses (%)
Adsorption	Pressure Swing Adsorption (PSA)	Vacuum	Water vapour, H_2S	4–7	2
Absorption	Water scrubbing	None; air stripping	None	7–10	<2
	Polyethylene glycol (PEG)	Air stripping	Water vapour, H_2S	7–10	<2
	Monoethanolamine (MEA)		H_2S	Atmospheric	<0.1
Membrane separation			Water vapour, H_2S	8–10	>10

Table 4 The performances of the various biogas upgrading technologies[24]

Process	Description	Advantages	Disadvantages
Adsorption	CO_2, higher C_xH_y, H_2S, Cl-components, odour will be removed by activated carbon/carbon molecular sieve	– High gas quality – Dry process – No use of chemicals – No process water demand – No waste water – Partial removal of N_2 and O_2 – No bacterial contamination of gas – Proven technology	– H_2S pretreatment – 3 to 4 parallel sheets needed – CH_4 level not stable – Complex process – High investment cost
Gas scrubbing	CO_2 and H_2S are absorbed by means of scrubbing fluid (*e.g.* water, amines, glycol ethane)	– High gas quality – Interesting investment costs – No pre-treatment necessary – Compact process – Proven technology – Re-use of CO_2 possible	– Disposal of waste water – Use of process water
Membrane process	CO_2 is separated due to the different permeation rate at the membrane	– Dry process – No chemicals – Low mechanical wear – Compact process	– Pre-treatment necessary – Low CH_4 recovery – High investment costs – High energy demand – Unstable long-term behaviours – Still few references
CO_2 liquefaction	CO_2 is liquefied by high pressure and low temperatures and separated in a rectification column due to the different permeation rate at the membrane	– Very high gas quality – No chemicals – No water – Compact process – Reuse of CO_2 possible	– Pre-treatment necessary – Very high energy consumption – High investment cost – Complex process – Only pilot plant reference

Table 5 Comparison of various biogas upgrading processes[24]

Process	Water scrubber	PEG scrubber	Amine scrubber	PSA	Membrane
CH_4-enrichment	High	High	High	Good	Low
O_2-/N_2-enrichment	Yes	Yes	Yes	No	Yes
CH_4-losses	Low	Medium	Low	Medium	High
Produced gas dryer required	Yes	Yes	Yes	No	No
H_2S pre-treatment required	No	Yes	Yes	Yes	Yes
Waste gas treatment required	No	Yes	Yes	No	No
Utility demand	Medium	High	High	Medium	High
Power demand	€0.25 m^{-3} biogas	€0.32 m^{-3} biogas	€0.42 m^{-3} biogas	€0.25 m^{-3} biogas	€0.50 m^{-3} biogas
Level of emission	Medium	Low	Medium	Low	Low
Capital cost	Medium	Medium	High	Medium	High

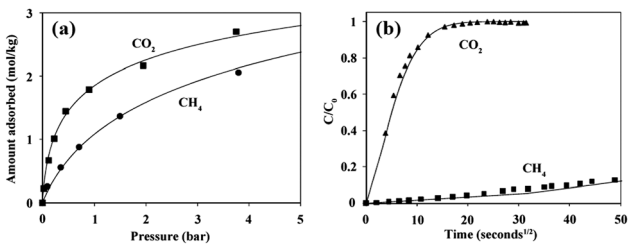

Fig. 4 Adsorption of CO_2 and CH_4 in carbon molecular sieve 3 K at 25 °C: (a) adsorption equilibrium; (b) uptake rate curves. Reprinted with permission from ref. 35. Copyright 2005 American Chemical Society.

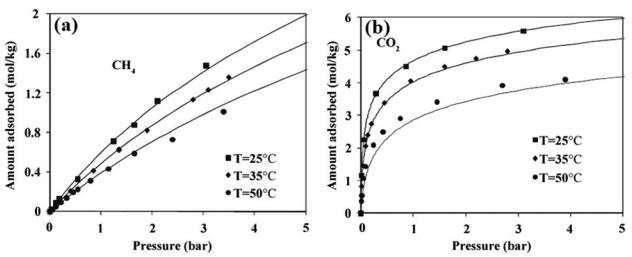

Fig. 5 Adsorption equilibrium of CH_4 (a) and CO_2 (b) on zeolite 13× at 25, 35 and 50 °C. Reprinted with permission from ref. 35. Copyright 2005 American Chemical Society.

Oxygen and nitrogen removal. Oxygen is normally not present in biogas since the facultative aerobic microorganisms in the digester would consume it. However, if there is air present in the digester nitrogen will still be present too in the gas when leaving the digester. These gases can be removed by adsorption using activated carbon, molecular sieves or membranes. They can also to some extent be removed in desulphurization processes or in some of the biogas upgrading processes.

Table 6 Summary of typical H_2S removal methods and their waste discharges[40]

Process	Detailed description
Precipitation	– A process in which hydrogen sulphide removal is based on the precipitation reaction between hydrogen sulphide and a metal ion in an aqueous solution. It involves addition of Fe^{2+} ions or Fe^{3+} ions in the form of *e.g.* $FeCl_2$, $FeCl_3$ or $FeSO_4$. The metal sulphide that is formed precipitates almost immediately and is removed together with the digestate. The metal ion is regenerated by using oxygen which converts the bounded sulphur to sulphur dioxide that can be used to produce sulphuric acid or gypsum. – The method is primarily used in digesters with high sulphur concentration as a first measure or in cases where H_2S in the biogas is allowed to be high (*e.g.* $\geq$1000 ppm). –The process is able to clean biogas down to less than 1 ppm hydrogen sulphide. It has so far been tested in a pilot plant (5 $Nm^3\ h^{-1}$), and will be available for biogas plants up to 1500 $Nm^3\ h^{-1}$.
Adsorption on adsorbents	– The hydrogen sulphide is adsorbed on the inner surfaces of engineered activated carbon with defined pore sizes on the inner surface. In order to increase the speed of the reaction and the total load, the activated carbon is either impregnated or doped (by the addition of a reactive species before the formation of the activated carbon) with permanganate or potassium iodide (KI), potassium carbonate (K_2CO_3) or zinc oxide (ZnO) as catalysers. – The H_2S removal is very efficient resulting in concentrations of less than 1 ppm. – Hydrogen sulphide can also be adsorbed using iron oxide-coated ($Fe(OH)_3$ or Fe_2O_3) support material (mostly pressed minerals, sometimes wood chips). In this treatment biogas is passed through iron oxide-coated material. Regeneration is possible for a limited number of times (until the surface is covered with natural sulphur), after which the tower filling has to be renewed. The process operates with two columns: one is absorbing, while the other is re-oxidized.
Chemical absorption	– Iron oxide is also used for hydrogen sulphide removal, of which the most common is iron sponge. The iron sponge reaction is given by the equation below. Other metals that may be used are zinc and sodium. $2Fe_2O_3 + 6H_2S \rightarrow 2Fe_2S_3 + 6H_2O$ (1) $2Fe_2S_3 + 3O_2 \rightarrow 2Fe_2O_3 + 3S_2$ (2)
Biological treatments	– Biological treatment of hydrogen sulfide typically involves passing the biogas through biologically active media. These treatments may include open bed soil filters, biofilters, fixed film bioscrubbers, suspended growth bioscrubbers and fluidized bed bioreactors. – Biological media work best in wet conditions, so moisture has to be removed before burning biogas in an energy generating process.
Water scrubbing	– Biogas (containing H_2S) feed is sent through a counterflow of water. Normally it is only used in combination with water scrubbing biogas-upgrading technologies. – The process can be designed as a regenerative process, in which case scrubbing water discharge would be significantly reduced. If the process is regenerative the desorbed gas will be vented out through an absorption filter of active carbon, iron hydroxide or iron oxide.

Both compounds are difficult (*i.e.* expensive) to remove; hence, their presence should be avoided unless the biogas is used for combined heat and power plants (CHPs) or boilers.

Ammonia removal. Ammonia is formed during the degradation of proteins. The amounts that are present in the gas are dependent upon the substrate composition and the pH in the digester. Apart from being corrosive on mechanical parts, the combustion of ammonia as a constituent of biogas leads to the formation of nitrogen oxides (NO_x). Since ammonia is soluble in water, its concentration can be further reduced by refrigerated water vapour removal methods as well as any water scrubbing technology where the biogas is passed through a counter flow of water. Neither of these systems introduces contaminants and only non-regenerative water scrubbing generates a waste discharge, *e.g.* scrubbing water to sewer. Ammonia is usually separated when the gas is dried or when it is upgraded. A separate cleaning step is therefore usually not necessary.

Water removal. Biogas is saturated with water vapour when it leaves the digester. The water vapour can condense in gas pipelines and together with sulphur oxides (acid) may cause corrosion of pipelines and the system. Removal of water from biogas can be achieved by increasing the pressure or decreasing the temperature causing condensation of the water from the biogas. Cooling can be achieved naturally by leading it through a pipe in the soil equipped with a condensate trap or with an electric cooler. Water can also be removed by adsorption using SiO_2, activated charcoal or molecular sieves. These materials are usually regenerated by heating and/or a decrease in pressure. Other technologies for water removal are absorption in glycol solutions or the use of hygroscopic salts, *etc*.

Removal of particulates. Particulates can be present in biogas and can cause mechanical wear in gas engines and gas turbines. Particulates that are present in the biogas have to be filtered out using 2 to 5 μm filters made of paper or fabric.

2. Metal–organic frameworks applied under atmospheric conditions

In most cases, MOFs have geometrically and crystallographically well-defined framework structures. These microporous crystalline

solids are composed of organic bridging ligands or "struts" coordinated to metal-base nodes to form a three-dimensional extended network with uniform pore diameters typically in the range 3 to 20 Å.[41–43] The nodes generally consist of one or more metal ions (*e.g.*, Al^{3+}, Cr^{3+}, Cu^{2+}, or Zn^{2+}) to which the organic bridging ligands coordinate through a specific functional group (*e.g.*, carboxylate, pyridyl). MOFs can be conceptually designed and synthesized based on how building blocks come together to form a net (an example is shown in Fig. 6).[44,45] Different synthetic approaches have been developed including solution reaction under ambient (r.t.) conditions, solvothermal synthesis (including hydrothermal synthesis), solid-state synthesis (so-called green synthesis), sonication assisted synthesis, and microwave synthesis.[46] A large variety of reported synthetic procedures encompass a wide range of temperature, solvent compositions, reagent ratios, reagent concentrations, and reaction times, and the fine-tuning of all of these parameters is crucial in optimizing the synthesis of the materials. Besides the generally used methods (such as solvent exchange followed by evacuation to remove guest molecules during sample activation), some advanced approaches for the purification (such as "density separation") and activation (such as "supercritical processing") of MOFs have been proposed and carried out, as highlighted in a recent review article.[47,48] Furthermore, to reach the full potential of these materials a complete activation of samples to produce uniform, empty pores is also an essential but often challenging task, especially for highly porous MOFs. Rigid MOFs usually have comparatively stable and robust porous frameworks with a permanent porosity, similar to zeolites, whereas flexible MOFs possess a dynamic, "soft" framework that responds to external stimuli, such as pressure, temperature, and guest molecules. From an application point of view, their extraordinary surface area,[49] fine tuneable pore surface properties,[50–52] and potential scalability to industrial scale[53] have made these materials an attractive target for further study. The intense current research efforts towards industrial applications of MOFs in gas storage, separation, and catalysis are attributed to their unique structural properties, including robustness, high thermal and chemical stability, unprecedented internal surface areas (higher than 10 000 $m^2\ g^{-1}$ (ref. 48)), high void volumes (55–90%), and low densities (from 0.21 to 1.00 g cm^{-3}), which can be maintained upon evacuation of the guest molecules from the pores.[54] Therefore, MOFs are considered to be versatile

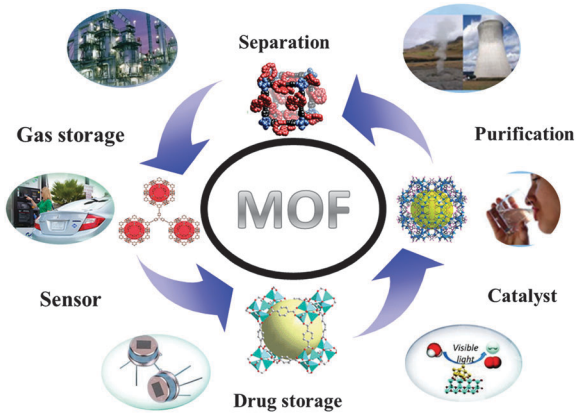

Fig. 7 Widespread potential applications of MOFs.

materials for widespread potential applications as illustrated in Fig. 7. The crystallinity of MOFs also allows precise structural characterization by diffraction methods, thus facilitating their rational design and the formulation of structure–function relationships. Besides the pre-design in synthesis, post-synthetic modifications have also been successfully used in tuning the pore properties of MOFs.[51]

MOFs hold several records among porous materials including highest surface areas,[51] hydrogen uptake ability based on physical adsorption, and methane and CO_2 storage capacity.[55–57] Recently, several thematic reviews have highlighted the rapid developments in the design, synthesis, and potential applications of these materials.[51,58–62] As porous materials, MOFs are therefore ideal adsorbents or membrane materials for gas storage and separation, including CO_2 capture, due to their large surface areas, adjustable pore sizes, and controllable pore surface properties. To date, a large number of different MOFs have been synthesized which have shown various promising applications in, for example, gas storage and separation, and so on. The rapidly growing number of related primary research articles (Fig. 8) is an indication that a comprehensive review in this field is necessary in order to draw general conclusions and provide some guided perspectives for future research, despite the fact that a few reviews involving related topics of CO_2 capture with MOFs have appeared.[63,64]

Similar to zeolites, MOFs can be built up from either tetrahedral or octahedral building blocks and have 3D microporous

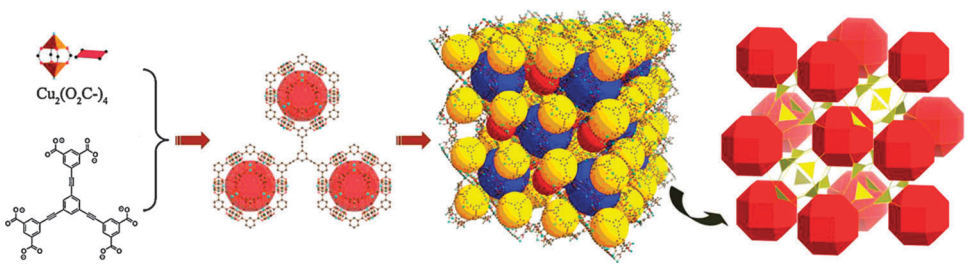

Fig. 6 MOF constructed from metal-containing nodes and bridging organic ligands to secondary building units (SBU) and the geometrical assembly of the framework with the ligands and polyhedral cages acting as three- (yellow) and twenty four- (red) connected nodes, respectively. Reprinted from ref. 44. Copyright 2011, with permission from Elsevier.

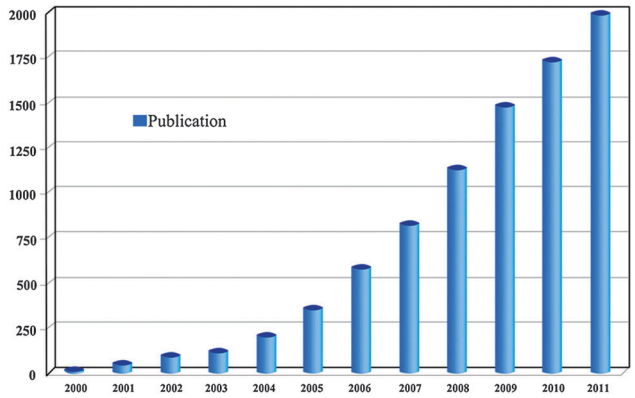

Fig. 8 Publications on "CO_2 adsorption and/or separation in MOFs" per year (Source: Thomson Reuters Web of Knowledge[SM]).

channels and ultrahigh specific surface areas. Due to the similarity in structure, MOFs are also called "organic" zeolites. However, by varying the linkers, ligands and metals in the material, their synthesis can be readily adapted to control pore connectivity, structure and dimension, featuring many opportunities of differences in functionality. The family of MOFs includes subsets such as isoreticular MOFs (IRMOFs),[54] zeolitic imidazolate frameworks (ZIFs),[65] and zeolite-like MOFs (ZMOFs).[66] Moreover, although covalent organic frameworks (COFs)[67] and porous organic polymers (POPs)[68] are not strictly MOFs, they are similar classes of materials because they are also made from building-block approaches.

The high surface area-to-weight ratio of MOFs is such that they have enhanced capacities for CO_2 capture at moderate pressures compared with zeolites. While zeolites possess higher storage capacities at pressures of less than 10 bar, it has been projected that their maximum capacities are limited to one-third of those of MOFs at pressures greater than 10 bar.[69] The capacities of metal–organic frames in the high pressure range increase with the amount of active area per weight unit: activated carbon has an active area of 400–1000 $m^2\ g^{-1}$, zeolites up to 1500 $m^2\ g^{-1}$, and frameworks between 1500 and 4500 $m^2\ g^{-1}$.[69]

2.1 Separation of the main gas components of biogas using MOFs

The production and utilization of biogas represent one of the most important routes towards reaching renewable energy targets and environment benefits. In order to use biogas, it needs to be cleaned or upgraded. Upgrading biogas requires a treatment whereby carbon dioxide is captured to separate it from methane. A lot of research efforts on CO_2 capture in these new adsorbent materials have been reported from experiments as well as from molecular simulation recently. Millward and Yaghi measured the adsorption capacity of CO_2 in a series of MOFs, experimentally, and found that the CO_2 uptake of MOF-177 reaches about 9 times the amount of CO_2 in a container without the adsorbent at room temperature and 35 bar.[70] Adsorption falls into two categories: (1) physical adsorption, which is temperature and pressure dependent (adsorption occurs at high pressures and low temperatures), and (2) chemical adsorption, where adsorption of CO_2 depends on the acid–base "neutralization" reaction (in this case caustic solvents are required). The adsorption isotherms of most solid adsorbents conform to a Langmuir-like shape, where at low partial CO_2 pressures, small changes in pressure result in large changes in capacity with a nearly linear slope. This is true for most MOFs investigated by Yaghi (Fig. 9),[70] where at low pressure (*ca.* 1 bar) MOF-74, MOF-505, and $Cu_3(BTC)_2$ had the highest capacities of the nine MOFs tested. At a pressure above 15 bars, MOF-177 outperformed the other tested MOFs, possessing nearly a double CO_2 adsorption capacity. The performance of CO_2 adsorbents is dependent on many factors such as pore size, pore shape and apparent surface area, thereby providing direct insight into the nature of the absorbent. Single-component gas adsorption isotherm data can further be used to estimate the adsorption selectivity for CO_2 over other gases, which is a crucial parameter that determines the purity of the capture and CO_2 selectivity. The lower-pressure (<1.2 bar) pure CO_2 adsorption capacities of metal–organic frameworks collected at ambient temperatures (20–40 °C) have been summarized in Table 7.[71,72a,b] The selective adsorption of CO_2 over CH_4 and N_2 in single-component (in most cases) and mixed-gas experiments for the reported MOFs has been summarized in Table 8.

There are published reports on comparisons of the separation properties of Mg-MOF-74 (ref. 67) with standard CO_2 capturing materials showing that this material represents a breakthrough for high-capacity storage under moderate regeneration conditions. The dynamic separation capacity, initial heat of interaction, and regeneration conditions for Mg-MOF-74 and several standard materials are compared in Table 9. Although dynamic separation capacity depends on experimental parameters such as flow rate and sample dimensions, Mg-MOF-74 is clearly a landmark among the MOFs, with a separation capacity more than twice the nearest candidate and far milder regeneration conditions in breakthrough experiments

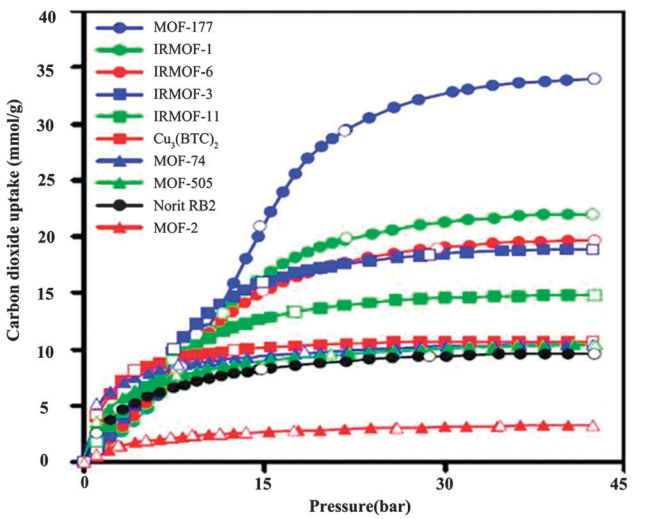

Fig. 9 Carbon dioxide adsorption isotherms at ambient temperature for MOFs reported by Yaghi *et al.* Reprinted with permission from ref. 70. Copyright 2005 American Chemical Society.

Table 7 Properties and CO_2 adsorption capacities of metal–organic framework adsorbents at 20–40 °C using pure CO_2

Chemical formula[a]	Surface area ($m^2\ g^{-1}$) BET	Langmuir	Temperature (°C)	Pressure (bar)	Capacity [b] (wt%)	Ref.
Mg(dobdc)	1174	1733	25	1	27.5	73
			25	1	27.2	74
	1800	2060	25	1	26.7	75
			25	1.1	26	76
	1495	1905	23	1	26	77
$Cu_3(BTC)_2(H_2O)1.5$			25	1	27	78
Co_2(dobdc)	957	1388	25	1	24.9	74
	1080		23	1	23.4	77
Ni_2(dobdc)	936	1356	25	1	23.9	74
	639		25	1	22.7	79
	1083	1312	30	1	22.6	80
	1070		23	1	20.4	77
Zn_2(dobdc)			23	1	19.8	77
			23	1	19.6	77
	816		25	1.1	17.6	70
$Cu_3(BTC)_2$	1400		20	1	19.8	81
		1492	25	1	18.4	78
			22	1	18.3	74
	1781		25	1	15.2	70
	1482		22	1	15	82
			25	0.8	10.6	79
			40	1	6.2	83
	857		22	1	6.2	82
$Cu_3(BTC)_3(H_2O)_3$			25	1	17.4	78
$Cu_3(TATB)_2$	3811	4436	25	1	15.9	84
$H_3[(Cu_4Cl)_3(BTTri)_8(mmen)_{12}]$	870		25	1	15.4	85
Co_2(adenine)$_2(CO_2CH_3)_2$	1040		25	1	15.2	86
$H_3[(Cu_4Cl)_3(BTTri)_8]$	1770	1900	25	1	14.3	87
Zn_2(ox)(atz)$_2$	782		20	1.2	14.3	88
Ni_2(2-amino-BDC)$_2$(DABCO)	1530		25	1	14	89
Cu_2(bdcppi)$(DMF)_2$	2300	2450	25	1	13.7	90
$Fe_3[(Fe_4Cl)_3(BTT)_8(MeOH)_4]_2$	2010		25	1	13.5	91
$Cu_3(TATB)_2$	2665	3065	25	1	13.4	84
$Cu(bpy)_2(BF_4)_2$			25	1	12.7	92
$Cu_2(bptc)(H_2O)_2(DMF)_3$	1547		25	1	12.6	70
Al(OH)(2-amino-BDC)	960		25	1	12	89
Al(OH)(bpydc)·0.97$Cu(BF_4)_2$	705		25	1	11.8	93
Cu_4(TDCPTM)$(H_2O)_4$	2620		20	1	11.7	94
Co(tImb)·DMF·H_2O	886	1170	25	1	11.7	95
Cu_2(TCM)		905	25	1	11.1	96
$Cu_3(BPT(N_2))_2$			25	2	10.8	74
Pd(μ-F-pymo-N^1,N^3)$_2$	600		20	0.86	10.7	97
Al(OH)(BDC)	1300		25	1	10.6	89
	1235	1627	30	1	9.2	98
$Cu_3(BPT)_2$			25	1	10.2	74
$Ni_2(BDC)_2$(DABCO)	1925		25	1	10	89
Ni_2(pbmp)			31	1	9.9	99
$Ni_3(pzdc)_2$(7*H*-ade)$_2(H_2O)_4$	165		25	1	9.8	100
Cu_2(TCM)		695	25	1	9.7	96
Cu(BDC-OH)(H_2O)	397	584	23	1	9.3	101
Fe(pz)Ni$(CN)_4$			25	1	9.3	102
Zn(nbIm)(nIm)	620		25	1	9.1	103
Zn(cnIm)(nIm)	1300		25	1	9.1	103
Zn(cyanIm)$_2$	960		25	1.1	8.8	104
Zn(IDC)	802		25	1	8.6	105
$Zn_4O(BDC)_3$	2304	2517	23	1	8.5	106
	2833		25	1.2	4.5	70
			25	1.1	4	107
	1892	2784	25	1	3.5	74
		1263	25	1	3.4	108
	3320	4140	25	1	3.2	109
Cr(OH)(BDC)			31	1	8.5	110
Ni_3(L-TMTA)$_2$(bpy)$_4$			25	1	8.2	111
$Zn_2(BDC)_2$(DABCO)			23	1	8.1	112
$V^{(IV)}O$(BDC)	600	872	25	1	8.1	74
In(OH)(BDC)	930		25	1	8	89
$Zn_4O(NO_2\text{-}BDC)_{1.19}((C_3H_5O)_2\text{-}BDC)_{1.07}[(C_7H_7O)\cdot BDC]_{0.74}$	1176	1400	25	1.1	7.7	109
$Zn_4(OH)_2$(1,2,4-BTC)$_2$	408		22	1	7.6	113
Pd(μ-H-pymo-N^1,N^3)$_2$	600		20	0.86	7.3	97

Table 7 (*continued*)

Chemical formula[a]	Surface area ($m^2\ g^{-1}$) BET	Langmuir	Temperature (°C)	Pressure (bar)	Capacity [b] (wt%)	Ref.
$Zn_4O(PDC)_3$	2096		25	1.1	7.3	70
Mn(pmdc)	410		20	0.9	7.3	114
$Pd(2\text{-pymo})_2$	600		20	0.86	7.3	115
Zn(cbIm)(nIm), (ZIF-69)	950	1070	25	1	8.6	103,116
Co(tImb)			25	1	7.2	95
Zn(brbIm)(nIm), (ZIF-81)	760		25	1	7.2	103
$Zn_4O(BTB)_2$			25	1	6.5	107
	5400	4690	25	1	3.6	75
	4508		25	1	3.4	70
			25	1	3.4	74
$Zn_8(ade)_4(BPDC)_6O{\cdot}2TEA$	1220		40	1	6.8	117
	1460		40	1	6.7	117
$Zn(almeIm)_2$	864		25	1	6.7	104
Zn(bIm)(nIm)	1090	1229	25	1	6.7	103,116
$Cu(pzdc)_2(bpy)$	633[c]		25	1	6.6	118
$Zn_2(bttb)(dpntcd)$			25	1	6.5	119
$Cu_2(pzdc)_2(pyz)$			27	1	6.4	120
Al(OH)(bpydc)	2160	2490	25	1	6.2	93
$Zn_2(NDC)_2(diPyNI){\cdot}Li$			25	1	6.2	121
Zn(mbIm)(nIm)	840		25	1	6.2	103
$Zn_4O[(C_7H_7O)_2\text{-BDC}]_{2.49}(NO2\text{-BDC})_{0.51}$	1020	1210	25	1.1	6.1	109
$Zn_2(NDC)_2(diPyNI)$			25	1	5.8	121
$Cu_4(O)(OH)_2(Me_2trzpba)_4$			25	1	5.8	122
$Zn_8(ade)_4(BPDC)_6O{\cdot}2TBA$	830		40	1	5.7	117
$Zn(Im)_{1.13}(nIm)_{0.87}$	1730	1970	25	1	5.7	103,116
$Cd_6(CPOM)_3(H_2O)_6$	231[c]		24	1	5.6	123
$H_3[(Cu_4Cl)_3(BTTri)_8(en)_{3.75}]$	345	376	25	1	5.5	87
In(OH)(BDC)	930		25	1	5.5	89
$Zn_2(TCPB)(DPG){\cdot}Li$			25	1	5.4	121
$Zn_4O(TPDC)_3$	1912		25	1	5.4	124
$Cu_2(hfbba)_2(3\text{-mepy})_2{\cdot}2DMF{\cdot}3\text{-mepy}$			20	1	5.3	125
$Zn_8(ade)_4(BPDC)_6O$	1680		40	1	5.2	117
$Zn_2(bpdc)_2(bpe)$	137.8[c]		25	1	5.2	126
$Zn_4O(BDC\text{-}NH_2)_3$	2160		1	1.1	5.1	70
			40	1	5	83
			25	1	4.7	74
$K_2(DABCO\text{-}H_2)[Zr(ox)_4]$			25	1	5.1	127
$Zn_2(bpy)(TCMO)$	1150		25	1	5	128
$Zn_2(TCMO)$			25	1	5	129
$Cu_2(TP)_3(OH)$	258	286	25	1	5	130
$Zn_2(TCPBDA)$	707	740	25	1	4.9	131
Cu(dImb)	435	579	25	1	4.7	132
$Zn_2(bpdc)_2(bpee)$			25	1	4.7	133
$Zn(hymeIm)_2$	1110		25	1	4.7	104
$Zn_4O(BDC\text{-}C_2H_4)_3$	2516		25	1.2	4.6	70
$Zn_2(TCPB)(DPG)$			25	1	4.6	121
$Zn(hymeIm)_2$	564		25	1.1	4.5	104
$Zn_2(bcphfp)$	378		25	1	4.5	134
$Zn(meIm)_2$	1135	1768	25	1	4.3	74
$Cr_3O(H_2O)_2F(BDC)_3$	2674		46	1	4.2	135
$Cu_2(hfbba)_2(3\text{-mepy})_2$			20	1	4.2	125
$Zn_3(OH)(p\text{-}CDC)_{2.5}$			25	1	4.1	136,137
$Zn_4O(BDC)(BTB)_{4.3}$	4034	5182	25	1	3.8	74
$Cu(2\text{-pymo})_2$	350		25	0.89	3.8	115
$Zn_20(cbIm)_{39}(OH)$	595	780	25	1	3.8	138
$Zn_2(hfbba)_2(3\text{-mepy})_2{\cdot}(3\text{-mepy})$			20	1	3.7	125
$Zn(cbIm)_2$	1050	1240	25	1	3.7	138
Cu(etz)			25	1	3.6	138,139
$Pd(\mu\text{-Br-pymo-}N^1,N^3)_2$			20	0.86	3.4	97
$Cd_2(ADA)_2(bpy)$			25	1	3.4	140
$Sc_2(BDC)_3$			30	1	3	141
$[Fe^{(III)}(Tp)(CN)_3]_2Co^{(II)}$	154		25	1	3	142
$Zn(dcIm)_2$	652		25	1	2.8	104
Mg(3,5-PDC)			25	1	2.7	143
$Cu(hfipbb)(H_2fipbb)_{0.5}$			25	1	2.6	144
$Zn_2(TCPBDA)(bpta)$	308		25	1	2.6	131
$Co_4(OH)_2(doborDC)_3$			25	1	2.6	145
$Zn_3(BDC)_3$	345		25	1	2.4	70
$Co(doborDC)_2$			25	1	2.4	145

Table 7 (*continued*)

Chemical formula[a]	Surface area (m^2 g^{-1}) BET	Langmuir	Temperature (°C)	Pressure (bar)	Capacity [b] (wt%)	Ref.
Pd(μ-I-pymo-N^1,N^3)$_2$			20	0.86	1.9	97
$Nd_6(OH)_9$(HSCA)(SCA)	13.45		31	1	1.9	146
Co(doborDC)$_2$(py)			25	1	1.6	145
$Zn_2(BDC)_2(H_2O)_2$			23	1	1.4	112
$Mn_2(ADA)_2$(bpy)			25	1	1.4	140
Ni(DBM)$_2$(bpy)			25	1	0.9	147
Cu(4-pymo)$_2$	65		20	1	0.8	115
Zn_3(Ge(4-carboxyphenyl)$_4$)$_2$	417.7		24	1	0.5	148

[a] See the list of abbreviations. [b] Capacities were estimated from adsorption isotherms in cases where the values were not specifically reported. [c] Surface area was calculated by CO_2 adsorption.

Table 8 Properties and CO_2 adsorption capacities of metal–organic framework adsorbents in mixed gases

Chemical formula[a]	Surface area (m^2 g^{-1})	Temperature (°C)	Pressure (bar)	Capacity[b] (mmol g^{-1})	Separation application	Ref.
$Zn_4O(NH_2bdc)_3$		27	28	68 wt%	CO_2–CH_4	149
$Sc_2(bdc)_3$		−38	1	0.9	CO_2–CH_4–H_2	141
			50	4.5	CO_2–CH_4–H_2	141
$Zn_2(bpdc)_2$(dpni)		−78	1	25.8	CO_2–CH_4	150
$Cu_2(BPnDC)_2$(bpy)		0	1	2.5	CO_2–CH_4	70
$Cu_3(btc)_2$	1270	25	6	10.9	CO_2–CH_4	151
			15	12.7	CO_2–CH_4	152
$Cr_3F(H_2O)_2O(btc)_3$	1900	30	48.7	18	CO_2–CH_4	153
Ni(pbmp)	169	31	1	2.5	CO_2–CH_4	99
			15	6	CO_2–CH_4–N_2	99
Mg_2(dobdc)	1174	25	0.1	23.6 wt%	CO_2–CH_4	154
			1	35.2 wt%	CO_2–CH_4	77
			50	63 wt%	CO_2–CH_4	76
$Zn_3(OH)$(*p*-cdc)$_{2.5}$		25	0.5	0.566	CO_2–CH_4	137
$Co_4(OH_2)_4(mtb)_2$		0	1	1.59	CO_2–CH_4–N_2	155
Ni(cyclam)$_2$(mtb)		−78	1	2.53	CO_2–CH_4–N_2	156
Mg(tcpbda)		25	1	1.49	CO_2–CH_4–N_2	157
Cr(OH)(bdc)			10	8.5	CO_2–CH_4	158
			5–10	2–3	CO_2–CH_4	158
Hydrated[Cr(OH)(bdc)]		31	18	7.7	CO_2–CH_4	159
Co(F-pymo)$_2$		0	20	7	CO_2–CH_4	160
Zn(F-pymo)$_2$		0	20	8	CO_2–CH_4	160
(Ni_2L1)(bptc)		25	1	9.3 wt%	CO_2–CH_4–N_2–H_2	160
(Ni_2L2)(bptc)		25	15	21 wt%		160
Zn_2(bttb)(py-CF_3)$_2$	390	25	0.15	0.2	CO_2–N_2	161
		25	18	3	CO_2–CH_4	161
Zn_2(bttb)		25	0.15	0.4	CO_2–N_2	161
		25	18	5	CO_2–CH_4	161
$[H_3O][Zn_2(\mu_3\text{-}OH)_3(bbs)_6$		0	1	2	CO_2–CH_4	161
Al(OH)(NH_2bdc)]	960	30	5	2.3	CO_2–CH_4	162
			13	6.7	CO_2–CH_4	162
Al(OH)(bdc)	1300	25	1	10 wt%	CO_2–CH_4	163
HCu[($Cu_4Cl)_3$(BTTri)$_3$(en)$_5$]	345	25	0.06	0.366	CO_2–N_2	87
			1	1.27	CO_2–N_2	87
HCu[($Cu_4Cl)_3$(BTTri)$_3$]	1770	25	0.06	0.277	CO_2–N_2	87
			1	3.24	CO_2–N_2	87

[a] See the list of abbreviations. [b] CO_2 adsorption capacities.

Table 9 Separation properties of Mg-MOF-74, other MOFs and current adsorbent materials

Materials	Separation capacity[a] (wt%)	Initial heat of adsorption (kJ mol^{-1})	Full regeneration conditions
Mg-MOF-74	8.9 (87%)	39	80 °C, purge flow
NaX	8.5 (71%)	43	11 °C, purge flow
MEA (30%)	13.4	84	120 °C, recirculation
Amino-MIL-53	3.7	—	159 °C, purge flow
ZIF-78	1.4	29	—

[a] Values in parentheses represent capacity regained after 10 min purge at 25 ml min^{-1}, indicating facile regeneration in Mg-MOF-74.

performed under similar conditions. Among the zeolites, NaX zeolite is among the most effective porous adsorbents considered for CO_2 separation.[164,165] Breakthrough experiments performed on NaX under identical conditions to those performed on Mg-MOF-74 show that the MOF materials with a dynamic capacity of 8.9 wt% CO_2 take up more CO_2 than NaX, which has a dynamic capacity of 8.5 wt%. Moreover, after a 10 min purge at 25 ml min^{-1}, NaX regains 71% of its capacity (6.4 wt%), whereas Mg-MOF-74 regains 87% of its capacity (7.8 wt%). The temperature required to achieve full regeneration in Mg-MOF-74 is also significantly reduced. Recently, Xiang and co-workers showed that a metal–organic framework (UTSA-16) displays a high uptake (160 cm^3 cm^{-3}) of CO_2 under ambient conditions.[166] In these calculations of partial pressures of CO_2 and CH_4, UTSA-16 has a higher selectivity than the other MOFs while it has a lower CO_2–CH_4 selectivity than Mg-MOF-74.

The application of MOF materials may boost new developments in adsorption technologies promoting up-scaling of industrial applications for gas molecules. Grande *et al.*, with the purpose of finding a suitable large-scale application of MOF materials, made extrudates of Cu-MOF linked by a binder to provide mechanical resistance.[167] Adsorption data of CO_2 and CH_4 at 30 °C are shown in Fig. 10. For evaluation purposes, they have made comparisons to CO_2 adsorption equilibrium on Cu-BTC powder at 25 °C.[70] The higher loading of CO_2 in the Cu-BTC pelletized sample compared to the powder form is due to a higher surface area. The surface area of the powder sample is 1781 m^2 g^{-1},[141] while the surface area of the pelletized sample is >2000 m^2 g^{-1}.[168] The material has a higher selectivity toward CO_2, decreasing at high pressures when the saturation plateau is reached.

In order to design and predict the structure of MOFs it is essential to understand how the frameworks are constructed and how they achieve the structural stability. Most of the porous MOFs are built upon metal clusters, so called secondary building units (SBUs). The SBUs serve as nodes and coordinate to organic linkers to form frameworks. Because of the large size of SBUs the resultant structures of MOFs are usually porous and could have relatively large pores. Introducing different sized organic linkers can also modify the pore size. Moreover, in general, longer and linear ligands give rise to frameworks with less stability.[169] The chemical and thermal stability of metal–organic frameworks is low due to relatively weak coordination bones that connect the metal and ligand components. Many MOFs require evacuation of the pores and since many MOFs are air- and moisture sensitive, careful handling under an inert atmosphere is needed if the best performance characteristics are to be obtained.[170,171]

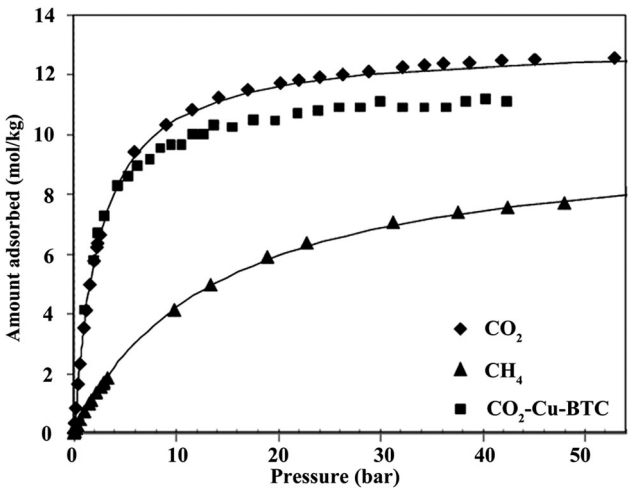

Fig. 10 High-pressure adsorption equilibrium of carbon dioxide (◆) and methane (▲) at 30 °C on MOF extrudates. For comparison, data for CO_2 on Cu-BTC powder (denoted by solid squares, ■) are presented. Solid lines are fittings of the data using the Langmuir model. Reprinted with permission from ref. 167. Copyright 2008 American Chemical Society.

2.2 Influence of the metal center on the CO_2 interaction

A broad range of ligand–metal center combinations are synthetically accessible as shown in Fig. 11[64,172] and thus MOFs can comprise an ideal palette for materials design and optimization, provided sufficient understanding of the CO_2 uptake mechanism is available (Section 3). MOFs exhibiting coordinatively unsaturated metal centers have been observed to provide an exceptional selectivity of CO_2 over N_2, which is determinant for an efficient gas separation.[76] Several studies have quantified how the CO_2 heat of adsorption changes when replacing the metal atom for a given MOF topology.[76,77,80,93,173] The coordination chemistry of metal cations especially of the d-block transition series is now very well developed and understood in terms of preferred ligands, donor-type geometries and stereochemistry such as Ag(I) can be linked through simple connecting ligand spacers to afford a one-dimensional chain structure. The two dimensional sheet constructions can be built using trigonal or square planer metal center nodes, while three dimensional architectures can be achieved by linking tetrahedral or octahedral metal centers with the same linear ligand spacers.[174]

Such studies exist wherein an isostructural MOF series has been explored to determine trends among various metal ions. Wade *et al.* performed such kind of investigation for the members of the $M_3(BTC)_2$ isostructural series (M = Cr, Ni, Cu, Mo, Ru) using improved activation procedures and syntheses.[175] In this series the heat of adsorption varied as Ni > Ru > Cu > Mo ≈ Cr. Despite the presence of BTC^{3-} guest anions in this structure, the material exhibited only a moderately decreased surface area *versus* the Cu, Cr, and Mo analogues. The differences observed among the remainder of the series

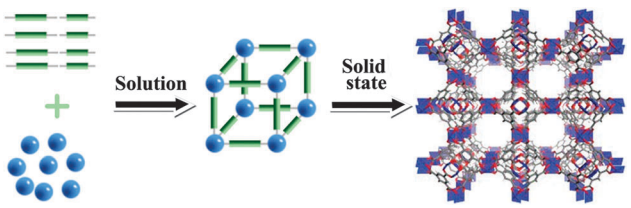

Fig. 11 Ligand and metal ion combination to synthesize metal–organic framework materials.

support the notion that metal identity affects the strength of the initial framework–CO_2 interaction. Due to the presence of donor guest molecules, it seems unlikely that the high enthalpy of adsorption observed for $Ni_3(BTC)_2$-$(Me_2NH)_2(H_2O)$ is due to metal–CO_2 interactions, and they speculated that the guests may play a role in the increased affinity. CO_2 adsorption isotherms were measured for the activated MOFs from 0–800 Torr at three temperatures over the 40–61 °C range. In striving for a diversity of metals in the M/DOBDC series, a search for a lighter and harder metal as a contrast to the late transition metals was started. One notable example to illustrate the effect of metal identity on the uptake is the family of materials known as MOF-74: M(DOBDC) (M = Mg, Co, Ni, Zn; DOBDC = 2,5-dioxy-1,4-benzene-dicarboxylate). Isotherms of CO_2 adsorption were measured at 23 °C to elucidate the effect of metal identity on the uptake in this isostructural series of materials (Fig. 12). The CO_2 adsorption isotherms measured at various temperatures revealed that the strength of the initial interaction varies as Mg > Ni > Co.[77] Heat of adsorption measurements show that Mg, Ni, and Co/DOBDC have an initial affinity of 47, 41 and 37 kJ mol^{-1}, respectively. Studies determined across isostructural series therefore provide important insight into the relative strength of the guest–framework interactions, which are a key to the efficient capture and release of CO_2. This interpretation is in agreement with the higher enthalpy reported for the more ionic Mg_2(DOBDC) (39–47 kJ mol^{-1}) *versus* the isostructural and softer Co (37 kJ mol^{-1}) and Ni (37–42 kJ mol^{-1}) derivatives.[77,80,154] The high value uptake may be attributed to the increased ionic character of the Mg–O bond. In this case, while Mg/DOBDC does not chemisorb CO_2, presumably because of the rigid nature of the framework that prevents insertion into the Mg–O bonds, the increased ionic character of this bond imparts additional uptake of the material for CO_2 beyond simple weight effects while maintaining the reversibility of adsorption.

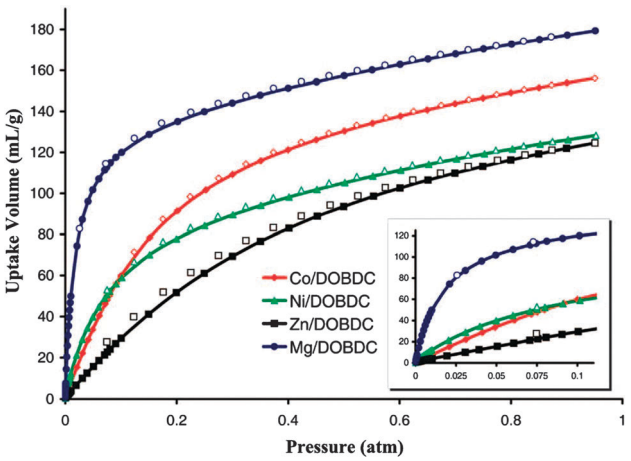

Fig. 12 Carbon dioxide sorption isotherm at 23 °C from 0 to 1 atm comparing the M/DOBDC series, along with an inset of the low pressure region (filled markers represent adsorption points; open markers represent desorption points). Reprinted with permission from ref. 77. Copyright 2008 American Chemical Society.

The interaction of CO_2, with accessible metal ion sites, has been simulated by applying DFT+D and B3LYP+D methods[173] for the M_2(dhtp) metal–organic frameworks (M = Mg^{2+}, Ni^{2+}, Zn^{2+}; dhtp = 2,5-dihydroxyterephthalate). The resulting sequence of binding energies for carbon dioxide adsorption on the open metal sites in the M_2(dhtp) metal–organic frameworks follows Mg > Ni > Zn.

The stability of the materials allows the removal of the solvent, which creates an open metal site. This site has a very high affinity for CO_2, which makes the material very promising for carbon capture. Often reasonable predictions on the ability of a material to adsorb CO_2 can be made using existing generic force fields.[176] For instance, the effect of metal ions on the CO_2 adsorption in two iso-structural MOFs, $M(4,4\text{-bipy})_2(OTf)_2$ (M = Cu and Co), has been investigated.[177] Changed metal ions resulted in different MOF structures and thus in diverse gas adsorption properties.

2.3 Influence of the ligand on the selectivity

A ligand is an ion or neutral molecule that bonds to a central metal atom or ion. Ligands usually contain O-, N- and S-donor atoms at their ''appendages'' so that they can strongly coordinate with the metal ion. Functional groups commonly seen in MOF ligands are carboxylates, carbonyls, amines, amides, thiols, cyano groups, *etc.* Attachment of the ligand to the metal may be through a single atom (monodentate ligand) or through two or more atoms (bidentate or polydentate ligand), Table 10.[178] Ligands containing only one functional group are called terminal ligands, because they discourage high dimensionality of the resulting MOF. Ligands act as Lewis bases (electron donors), while the central metals they bond to act as Lewis acids (electron acceptors). Ligands have at least one donor atom with a pair of lone electrons used to form coordinative covalent bonds with the central metal ion or atom that they are attached to. The space between the functional groups, or the ''body'' of the ligand, is also very important. The body creates the pore walls and is a key factor in MOF stability. Therefore, it is of no surprise that aromatic rings, such as benzene rings, are commonly incorporated into the ligand body.[179]

Given the wide variety of ligands available through conventional synthesis, there is significant opportunity to tune CO_2–MOF interactions using different ligands. Wade *et al.* have

Table 10 Examples of mono-, bi-, tri- and polydentate ligands

Ligand type	Examples
Monodentate	Pyridine, C_5H_5N Aqua, OH_2 Hydroxo, OH^- Chloro, Cl^-
Bidentate	Acetylacetonato $(CH_3COCHCOCH_3)^-$ Bipyridine Ethylenediamine, $H_2NCH_2CH_2NH_2$ Oxalato, $C_2O_4^{2}$
Tridentate	Diethylenetriamine, $NH(CH_2CH_2NH_2)_2$
Polydentate	$EDTA^{4-}$ (sexidentate, binding *via* nitrogen and oxygen), triaminoethylamine, $N(CH_2CH_2NH_2)_3$ (tetradentate, binding *via* nitrogen)

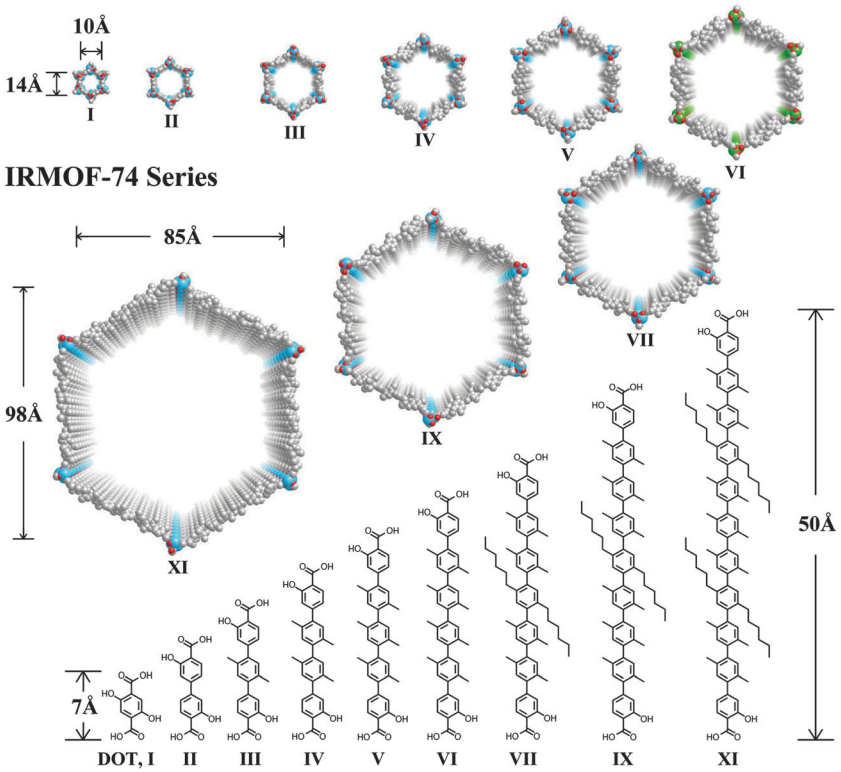

Fig. 13 Perspective views of crystal structures of the IRMOF series describing pore aperture and chemical structure of organic links used in the synthesis. From ref. 183. Reprinted with permission from AAAS.

been fascinated by the bridging ligands of the $M_3(BTC)_2$ members which remains an underexplored and open question. A potential interaction between CO_2 and the Lewis basic BTC^{3-} anions residing in the $[Ru_3(BTC)_2]$ may contribute to the observed increase in adsorption enthalpy here.[175] Overall, these results suggest that the use of more electropositive divalent metals, such as Mg^{2+}, or incorporation of more highly charged dimetal units could lead to $M_3(BTC)_2$ analogues with increased CO_2 affinity at low coverage. Babarao and Jiang simulated the storage of CO_2 in a series of MOFs at room temperature, and reported that the organic linker plays a critical role in tuning the free volume and accessible surface area and determining CO_2 uptake at high pressures.[180] Torrisi *et al.* using DFT calculations examined the intermolecular interactions between CO_2 and a series of functionalized aromatic molecules. The results clearly showed that the strength of CO_2–aromatic ring interactions could be tuned by introducing some functional groups to the ring structure.[181,182] Halogen substituents exhibit a relatively strong destabilization effect, whereas methyl groups are able to slightly improve the stability, primarily due to the strengthened-quadrupole interaction arising from the inductive effect. Bae *et al.* synthesized a mixed-ligand MOF, $Zn_2(NDC)_2(DPNI)$, and found that this material shows a selectivity of $\sim$30 for CO_2 over CH_4 by using the ideal adsorbed solution theory (IAST).[10]

One of the most significant factors for adsorption is pore size (Section 5.1) which has been studied by Deng *et al.* applying various ligands.[183] They reported that the systematic expansion of a well-known MOF structure, MOF-74, from its original link of one phenylene ring (I) to two, three, four, five, six, seven, nine, and eleven (II to XI, respectively), as shown in Fig. 13, afforded an isoreticular series of MOF-74 structures (termed IRMOF-74-I to XI) with pore apertures ranging from 14 to 98 Å. The pore size can separate the two gases by a molecular sieving effect (or a steric effect). Several MOFs have shown selective adsorption of CO_2 over N_2 or CH_4 by the molecular sieving effect.[86,184–186]

3. Separation mechanisms of the biogas components in MOFs

Physical adsorption on solids possesses significant advantages for energy efficiency compared with chemical adsorption approaches. CO_2 molecules dissolve into the bulk of the material, and CO_2 adsorption involves either physisorption (van der Waals) or chemisorption (covalent bonding) interactions between the gas molecules and the surface of a material. The CO_2-laden solid is purified in stages using pressure, vacuum, or temperature swing adsorption cycles to remove and concentrate the CO_2. Several authoritative review articles have discussed the characteristics and examples of physical adsorbents.[21,63,187]

As a result, only a limited number of MOFs have been assessed for their adsorptive separation performances, and the influencing factors as well as their separate and cooperative contributions are

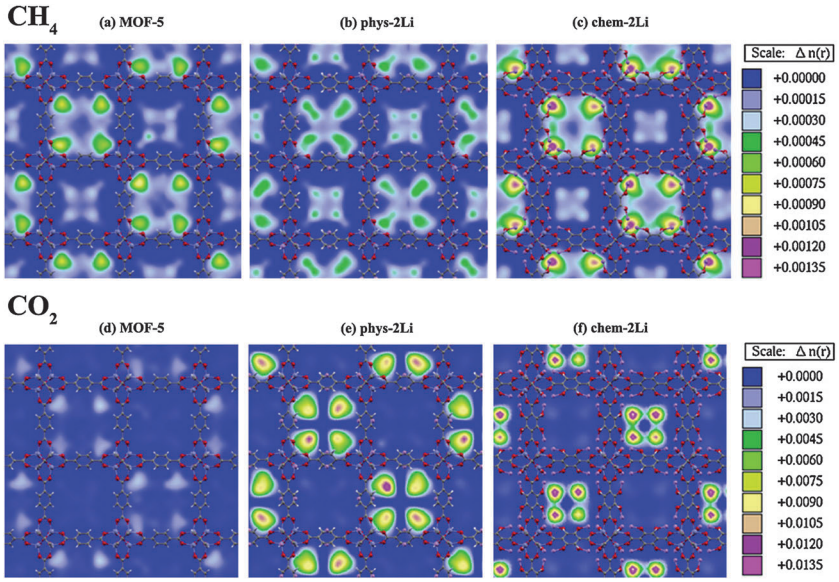

Fig. 14 Contour plots of the center of mass probability densities of CH_4 and CO_2 at 0.1 MPa in MOF-5 (Zn, blue; O, red; C, gray, H, white and Li, purple). Reproduced from ref. 188.

not quite clear. Computer modelling provides a useful complement or alternative for mixture separation study in MOFs. With the development of computational theory and method, molecular modelling can achieve accurate predictions of mixture adsorption, even for highly non-ideal mixtures and complex adsorbents, and has been widely used to study mixture separation in other nanoporous materials. This method can provide deep insights into the underlying mechanisms that control adsorption and selectivity of mixtures in nanoporous materials at the molecular level, as well as the cooperative effects of a set of selected factors. This information is difficult to obtain experimentally, while it is very important in understanding the gas separation performance of MOFs, and thus important for designing new MOFs with improved separation performance for targeted applications. However, because the CO_2 partial pressure in biogas is nearly 1 bar, it is of greater importance to understand CO_2 adsorption in MOF materials in the sub-atmospheric pressure region than at high pressure. Xu *et al.* elucidated the mechanisms at the molecular level in Li-modified MOFs by Grand Canonical Monte Carlo (GCMC) simulations and Density Functional Theory (DFT) calculations and concluded that the preferential adsorption sites for CH_4 in MOFs are all around the corner regions formed by ZnO_4 clusters (as can be seen from Fig. 14 when a CO_2–CH_4 mixture with a gas composition of 10% CO_2 and 90% CH_4 in the three MOFs at 0.1 MPa was used). However, the center of mass probability densities of CO_2 shown in Fig. 14 (it should be pointed out that here the density of CO_2 in MOF-5 is increased by 10 times for visualization and CH_4 was omitted in all the cases for clarity) demonstrate that the preferential adsorption sites for CO_2 are around the corners for MOF-5 in physical doping (phys-2Li), while in chemical doping (chem-2Li) the linkers become the preferential adsorption sites.[188]

Accompanied by molecular simulation studies, X-ray diffraction, IR spectroscopy (coupled adsorption), *etc*. have proven to be useful techniques in probing CO_2 adsorption sites in MOFs. Bordiga *et al.* investigated the CO_2 adsorption in HKUST-1 by IR spectroscopy and their results showed that the coordinatively unsaturated Cu(II) centers in this MOF act as specific interaction sites and play an important role in the adsorption.[189] Similarly, Blom *et al.* have shown that CO_2 adopts the end-on coordination mode when interacting with the coordinatively unsaturated nickel sites of Ni_2(dhtp) (H_4dhtp = 2,5-dihydroxyterephthalic acid), which gives rise to high CO_2 adsorption capacity at low pressures and ambient temperatures.[80] Vimont *et al.* studied the CO_2 adsorption mode at low coverage in MIL-53(Cr). The red shift of the ν_3 band and splitting of the ν_2 mode of CO_2 in addition to the shifts of the ν(OH) and the δ(OH) bands of the MIL-53(Cr) hydroxyl groups provide evidence that CO_2 interacts with the O atoms of framework –OH groups as an electron-acceptor *via* its carbon atom.[177]

The mechanism of capture is often based on physisorption, and involves weak interactions between the adsorbent and CO_2 molecules (rather than chemical bonds), with heats of adsorption of around -11 kJ mol^{-1}.[190,191] A key concern for physical adsorbents is balancing a strong affinity for removing an undesired component from a gas mixture with the energy consumption required for their regeneration. In addition to the adsorption capacity, the selectivity is a principal property relevant to adsorptive gas separation. While both factors are dependent on the operational temperature and pressure, as well as the nature of the adsorbent and the gas adsorbate, the factors influencing selectivity are more complicated. The possible mechanism of adsorptive separation includes (1) the molecular sieving effect, which is based upon size/shape exclusion of certain components of a gas mixture; (2) the thermodynamic equilibrium effect, due to the preferential adsorbate–surface or adsorbate packing interaction; and (3) the kinetic effect, due to differences in the diffusion rates of different components of a gas mixture.[58]

4. Upgrading selectivity of gas mixtures on MOFs

From an industrial point of view, gas separation is one of the most attractive research fields in MOFs, which it is believed to be one of the fields in which the first application of MOFs was performed.[38,192] A key step in designing an adsorption process for the separation and purification of CO_2 is the selection of a highly selective adsorbent with a high CO_2 capacity. The best way to evaluate MOFs for large-scale CO_2 separation and capture is undoubtedly to test the materials under mixture conditions by measuring the column dynamics from breakthrough measurements. Unfortunately only a few MOFs have been already tested by packed-column methods.[116,138,162,193] However, these breakthrough measurements require a specially designed experimental system. Measurements of equilibrium mixture isotherms sound straightforward but they are tedious in practice and require additional measurements for determining the compositions of both gas and adsorbed phases. Thus, until now, most studies on CO_2 separation and capture using MOFs have reported single-component isotherms of CO_2 and CH_4 and were well summarized.[194] However, the study on MOFs as adsorbents in gas separation is still in its early stage up to now.[58] From an experimental point of view, multicomponent adsorption measurements in MOFs are expensive and time-consuming, similar to other nanoporous materials, although the measurements of single-component adsorption are relatively straightforward.[195]

Recent efforts have been devoted to develop these materials for the separation and capture of CO_2. Two common strategies for enhancing the CO_2 affinity and selectivity in MOFs include functionalization of the frameworks with amines or other basic groups and removal of terminal bound solvent molecules to expose coordinative unsaturated metal centers (UMCs). The former relies on chemisorptive interactions inspired by liquid amine scrubbers,[196] while the benefit of the latter is commonly ascribed to a physisorptive process enhanced by ion induced dipole interactions.[197] Yang and Zhong performed a systematic computational study towards the molecular understanding of the characteristics for the separation of CO_2–CH_4–H_2 mixtures in metal–organic frameworks MOF-5 (IRMOF-1) and Cu-BTC.[198] They found that both geometry and pore size affect largely the separation efficiency. Furthermore, the electrostatic interaction was found to enhance greatly the separation efficiency of mixtures composed of components with different chemistries, which correlates with the results of Babarao *et al.* Xu *et al.* greatly improved the separation of CO_2–CH_4 mixture gas in Li-modified MOF-5 by physical and chemical doping. Owing to the enhancement of electrostatic potentials by the presence of the metals, adsorption selectivity was predicted to be much higher than in MOF-5 as shown in Fig. 15.[188,199] The strategy is applicable to the separation of other gas mixtures with components that have large differences in dipole and/or quadrupole moments. Moreover, Lan *et al.* investigated in a comprehensive manner the effect of doping of a series of alkali, alkaline earth, and transition (Sc and Ti) metals in nanoporous

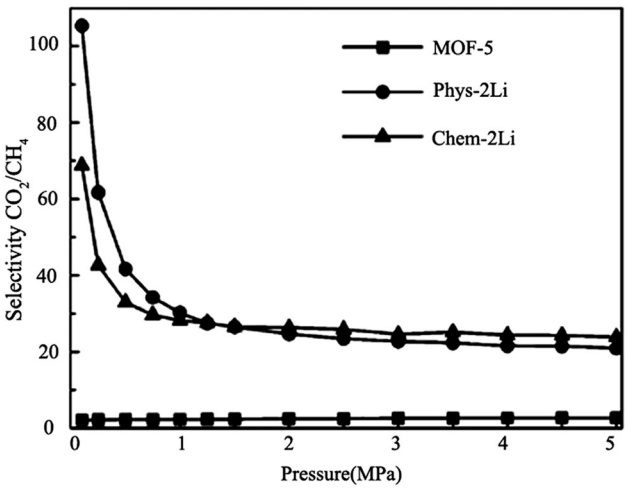

Fig. 15 The calculations were performed at 25 °C with the pressure range of 0.1–5 MPa and mixture composition of 10% CO_2 and 90% CH_4. Reproduced from ref. 188.

covalent organic frameworks (COFs) on CO_2 capture.[200] The result indicates that, among all the metals studied, Li, Sc, and Ti can improve the uptake of CO_2 in COFs significantly. However, the binding energy of a CO_2 molecule with Sc and Ti exceeds the lower limit of chemisorption and, thus, suffers from the difficulty of desorption. From the comparative studies above, it is found that Li is the best surface modifier of COFs for CO_2 capture among all the metals studied. As the pressure increases to 40 bar, the CO_2 uptake of the Li-doped COF-102 and COF-105 reaches 1349 and 2266 mg g^{-1} at 25 °C, respectively. The simulated gravimetric CO_2 uptake for non-doped and Li-doped COFs at representative pressures is summarized in Table 11 together with the data for several MOFs with high CO_2 uptake for comparison. Recently, Bae *et al.* reported that by exchanging the hydroxyl protons with Li cations in the non-catenated MOF framework (Zn_2(TCPB)(DPG)), the CO_2–CH_4 selectivity increased significantly at low pressures because of an increased interaction strength between CO_2 and the framework.[121]

A family of mixed-ligand MOFs exhibiting a permanent microporosity has been reported too.[150] The use of two different linkers opens up more possibilities to tune pore size and chemical functionalities independently. Youn-Sang Bae *et al.* using a combination of experimental measurements and the ideal adsorbed solution theory (IAST) observed in a mixed-ligand paddle-wheel MOF an improved selectivity for a CO_2–CH_4 mixture.[10]

Table 11 Comparison of CO_2 uptake (mg g^{-1}) in porous materials at 0 °C[200]

Materials	P = 1 bar	P = 10 bar	P = 40 bar
COF-102	52	685	1197
Li-COF-102	409	1092	1349
COF-105	93	554	1773
Li-COF-105	344	948	2266
MOF-5	44	479	970
MOF-177	35	497	1490
IRMOF-6	41	487	870
MIL-101(Cr)	190	630	1760 (30 °C, 50 bar)

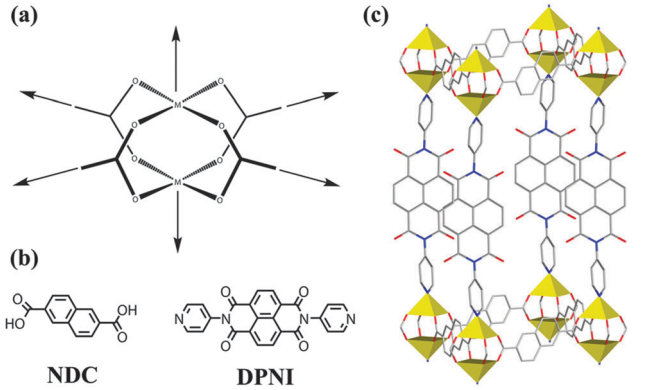

Fig. 16 (a) Mixed-ligand paddlewheel coordination geometry (M = Zn). (b) Chemical structure of MOF ligands NDC and DPNI. (c) Single crystal structure. Grey represents carbon, blue nitrogen, red oxygen, and yellow polyhedra represent Zn clusters. Reprinted with permission from ref. 10. Copyright 2008 American Chemical Society.

These MOFs contain carboxylate-terminated linkers in two directions to define two-dimensional sheets that are pillared by pyridyl linkers in the third dimension as shown in Fig. 16. The selectivities reported for CO_2 and methane were verified by GCMC simulations.

5. Strategies to improve the CO_2 capture and selectivity of MOFs applied in mixtures

Because of the great variety in the chemical composition of MOFs, the adsorptive separation performances of MOFs are more complicated due to the interplay of various factors. To date, many attempts have been made for improving the ability of MOFs to selectively adsorb CO_2. In the following paragraphs, we briefly review several bottom-up strategies that have been proposed to tune CO_2 capitation performance. These strategies are for example pore-size control, open metal sites, polar function groups, and introduction of alkali-metal cations.

5.1 Pore-size and catenation control

One of the most important factors for gas adsorptive separation processes by microporous materials is the pore size. When the pore size of a material is located between the kinetic diameters of two gas molecules as summarised in Table 12 (*e.g.* CO_2: 3.3 Å; CH_4: 3.8 Å), one can separate the two gases by a molecular sieving effect (or a steric effect). If the pores possess the right size, only the smaller molecule (CO_2) can diffuse into the pores, whereas the larger molecule (CH_4) is totally excluded. If the pore size is slightly larger than the kinetic diameter of the larger molecule (CH_4), one can separate the two gases in a kinetic way, which is achieved by the difference in diffusion rates since the larger molecule (CH_4) diffuses slower than the smaller molecule (CO_2). When the pore size is large enough so that both molecules can readily diffuse into the pores, the two molecules may be separated by differences in their equilibrium adsorption, which is used in a large majority of adsorptive separation processes. Even for separation processes based on differences in equilibrium adsorption, the pore size may play a role in dictating the adsorbed amount. In most cases, pores that are too large do not show good gas separation properties. Several MOFs have shown selective adsorption of CO_2 over N_2 or CH_4 by the molecular sieving effect,[86,184,186] and a few MOFs have exhibited selective CO_2 adsorption by the kinetic separation effect.[161,201] Other than these cases, most reports of selective CO_2 adsorption in MOFs are because of differences in the equilibrium adsorption, in which the relative interactions between the adsorbate (CO_2, CH_4, or N_2) and the MOF atoms are most important.

Table 12 Properties of biogas components

Gas properties	Methane	Carbon dioxide	Nitrogen
Molecular weight (g mol^{-1})	16	44	28
Molecular size (Å)	3.8	3.3	3.6
Polarizability $\times 10^{25}$ cm^3	26.0	26.3	17.6
Quadrupole moment $\times 10^{40}$ C m^2	0.0	14.3	1.52
Dipole moment $\times 10^{-18}$ esu cm	0.0	0.0	0.0

Düren and Snurr studied the effect of the length of organic linkers on the selectivity for a methane–*n*-butane mixture in five IRMOFs with similar chemistry and topology but with different pore sizes.[202] Their simulation results show that the selectivity for *n*-butane increases with decreasing cavity size as well as with increasing number of carbon atoms in the linker molecule. The simulation results of Yang and Zhong show that the difference in the structure of the two MOF materials is responsible for the different selectivity, with IRMOF-1 possessing a crystal structure with large cubic pores, whereas Cu-BTC has a pocket/channel structure (5.0 and 9.0 Å, respectively) as shown in Fig. 17.[198] Due to the electrostatic interactions between adsorbates and MOFs, the energetic effect is predominant, leading to a slight increase of selectivity with rising pressure. However, the smaller pore sizes in Cu-BTC induce stronger confinement effects, and the packing effect occurs at lower pressure (loading). For CO_2–CH_4 mixtures it was observed that selectivity enhances quickly with increasing pressure in the low-pressure region, followed by nearly independent steps at high pressures. This microscopic behaviour can be explained since the dynamic sizes of CO_2 and CH_4 are comparative, the packing effect is nearly identical for both gases, and the energetic effects become the predominant influencing factor in the whole pressure range. Martín-Calvo *et al.* studied the separation of the natural gas components in IRMOF-1 and Cu-BTC, including CH_4, CO_2, C_2H_6, C_3H_8 and N_2, and also found that the pocket/channel structure in Cu-BTC largely affects the separation efficiency.[203]

In addition to the size and shape (catenation) of the pores in MOFs, important factors that influence largely the separation performance of MOFs for a certain gas mixture, a suitable pore size that leads to strong confinement effects to induce large differences in adsorbate–adsorbent interactions, is crucial to create high selectivity. Greathouse *et al.* investigated the separation of noble gases in IRMOF-1, and found that when Xe is mixed with smaller atoms (Ar) the selectivity for Xe is larger

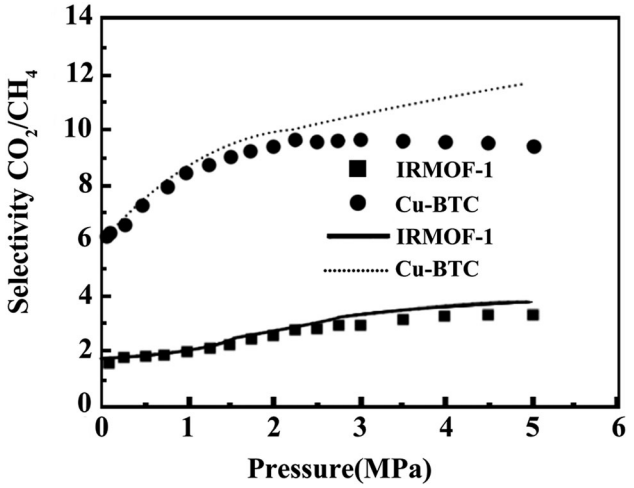

Fig. 17 Selectivity for equimolar gas mixtures in IRMOF-1 and Cu-BTC at 25 °C. Reprinted with permission from ref. 198. Copyright 2005 American Chemical Society.

than that in the mixture with larger atoms (Kr).[204] The optimization of MOFs for gas separation should involve the examination of the atomic properties of both feed gas and the substrate. The catenated structure in IRMOFs can be generated in different types of pores and thus induces larger differences in the adsorbate–IRMOF framework interactions between different components.[205] Similar results have been found for CO_2–N_2 and CH_4–N_2 mixtures in these MOFs, as well as for CO_2–CH_4 and both C_4 and C_5-alkane isomer mixtures in the catenated MOFs of IRMOF-13 and PCN-6 and their non-catenated counterparts, IRMOF-14 and PCN-60.[199,206] Moreover, the selectivity behaviour in catenated IRMOFs is more complicated, with a common trend in all the examined gas compositions: a rapid decrease of selectivity is observed at low pressures, which becomes more pronounced with increasing CH_4 or CO_2 concentration.[205] In addition, Gallo and Glossman-Mitnik also discussed the enhancement of the catenated structure on the selectivity by calculating the energetic interactions between adsorbate and framework.[207]

One additional method using mixed ligands to make solid solutions of MOFs is also a strategy that has been used to modify the pore size. Although there are several reports on this approach, a clear relationship between the mixture level of the ligands, resulting pore size, and consequent separation performance is difficult to address. Since it is difficult to finely control the pore size by this method, tuning separation properties could be a viable option in some MOFs, potentially clearing a new path in this field. In all of these approaches, it is clear that subtle pore control is very important for these kinds of materials to be able to execute highly selective separation.[109,208]

5.2 Open metal sites

Metal atoms in most MOFs are coordinatively saturated by framework components, but in certain MOFs some of the metal atoms are partially coordinated by guest solvent molecules. When these coordinated solvent molecules are removed by heating the material, coordinatively unsaturated metal sites are created within the MOF pores. The open metal site strategy has been explored as a means for improving the affinity and selectivity of metal–organic frameworks *via* the generation of structure types bearing exposed metal cation sites on the pore surface. Besides large surface areas and pore volumes they are advantageous for conducting host–guest chemistry such as catalysis, therefore mesoporous (openings between 20 and 500 Å) or even macroporous (openings greater than 500 Å) materials are attractive. Microporous materials have pores less than 20 Å which results in strong interactions between gas molecules and the pore walls making them good candidates for gas storage and gas separation applications. In all cases, measurements of these openings are done from atom to atom while subtracting the van der Waals radii to give the space available for access by guest molecules. Although MOFs can be constructed with ligands, designed to generate large pores, frameworks will often interpenetrate one another to maximize packing efficiency.[209] In such cases, the pores sizes are greatly reduced, but this may be beneficial for some applications. Indeed interpenetrated frameworks have been intentionally formed and found to lead to improved performance, for example, in H_2 storage.[210] These open metal sites have been widely studied for improving H_2 storage in MOFs and increasing the heat of adsorption (Q_{st}).[136,211–213] They have also been shown to be promising for improved CO_2 capture and separation. For example, Bae *et al.* compared the CO_2–CH_4 selectivities between carborane-based MOFs with and without open metal sites, and the results suggested that open metal sites in a MOF could aid in the separation of (quadru) polar–nonpolar pairs such as CO_2–CH_4.[137] A series of isostructural frameworks $[M_2(dhtp)(H_2O)_2]$ (H_4dhtp: 2,5-dihydroxyterephthalic acid; M = Zn, Ni, Co, Mg, Mn) are also denoted M-MOF-74,[151] CPO-27-M,[137] and M/DOBDC,[77] with 1D-hexagonal channels of around 11 to 12 Å shown to have high concentrations of metal sites after the removal of coordinated H_2O molecules. This series of MOFs showed high CO_2 uptake especially at low pressures (0.1–0.2 bar).[77,154] Also, these MOFs have high Q_{st} values for CO_2 (37–47 kJ mol^{-1}), which suggests preferential adsorption of CO_2 on open metal sites. To confirm this, Dietzel *et al.* obtained an X-ray single-crystal structure of CO_2 bound ''end-on'' to the open metal sites in Ni-MOF-74, which clearly shows the role of the open metal sites in CO_2 binding.[80] Hence, these MOFs are considered some of the most promising MOFs for CO_2 capture and separation. Another interesting feature of these MOFs is that they can be made with different metals; among this series, the MOF with Mg showed the highest CO_2 uptake as well as the highest Q_{st} value for CO_2.[77] Yazaydin *et al.* noted that one reason why Mg-MOF-74 shows better CO_2 adsorption than other MOFs containing open metal sites is the higher density of open metal sites in Mg-MOF-74. Yazaydin *et al.*[214] screened 14 MOFs with open metal sites for CO_2 capture from flue gas using a combined modelling and experimental approach. The simulations indicated that the ionic character of the metal–O bonds promotes higher CO_2 uptake. Thus, it is believed that MOFs having a high density of open metal sites are promising

in terms of either per unit of surface area or per unit of free volume of material. Gallo *et al.* reported that the open metal sites in MOF-74 may improve the separation capability of a CH_4–H_2 mixture by calculating the energetic interactions between the sorbate and the framework.[207] The strong $Zn^{\delta+}$–$O^{\delta-}$ dipoles on the surface were shown to be responsible for the strong energetic interaction with the adsorbates, improving the separation capability.

The earliest studies on the open metal site effect of MOFs were performed predominantly on $Cu(BTC)_2$(HKUST-1).[215] These sites interact more strongly with CO_2 due to the high charge density of the Cu^{2+} cation, resulting in a zero-coverage isosteric heat of adsorption of -29.2 kJ mol^{-1}. A number of independent studies have reported the adsorption isotherms for this compound, wherein adsorption capacities range from 15.0 to 18.4 wt% at 1 bar and 25 °C.[70,78,79,81] The difference in these values likely stems from the degree of purity of the material or the degree of activation (desolvation) of the compound. Note that the adsorption properties of metal–organic frameworks containing bound solvent molecules are highly dependent upon the desolvation conditions. Furthermore, careful handling of the materials following activation is essential, as a result of the propensity of the open metal sites to become hydrated due to even a brief exposure to atmospheric moisture.[216]

5.3 Polar functional groups

One of the most attractive properties of MOFs is the possibility to tailor the functionality by exploiting the richness of organic chemistry giving rise to high adsorption selectivities and capacities and yet minimizing the regeneration energy. Efforts to provide desired surface properties of MOFs can be divided into two main strategies: (1) direct assembly and (2) post-synthesis modification.[51] The first strategy is the direct assembly of new MOFs from particular metal nodes and organic linkers with specific functionalities. As an example, Yaghi and co-workers synthesized a series of zeolite imidazolate frameworks (ZIFs) with the gmelinite (zeolite code GME) topology.[103] By changing the imidazole linker, they produced a wide range of pore metrics and functionalities for a CO_2 separation process; the imidazole link functionality was altered from polar (–NO_2, ZIF-78; –CN, ZIF-82; –Br, ZIF-81; –Cl, ZIF-69) to nonpolar (–C_6H_6, ZIF-68; –CH_3, ZIF-79). The order of CO_2 uptake at 1 bar and 25 °C was in line with the greater attractions expected between the polar functional groups in the ZIFs and the strongly quadrupolar CO_2. Also, ZIF-78 and ZIF-82 showed higher CO_2–CH_4 selectivities than the other ZIFs because these ZIFs have greater dipole moments than the other functional groups. Another example of direct assembly of new MOFs is the cobalt-adenine MOF named bio-MOF-11. Rosi and co-workers synthesized this MOF based on the idea that the multiple Lewis basic sites of adenine, including an amino group and pyrimidine nitrogen, should have a strong interaction with CO_2.[86] The gas adsorption results showed high CO_2 uptake at 25 °C. Also, this material showed a high Q_{st} value for CO_2, which is similar to values for some other amine-functionalized MOFs. Similarly, amine-functionalized MIL-53(Al) showed a significant increase in the CO_2–CH_4 separation factor compared to the non-functionalized MOF.[162,217] In addition, the amine-MIL-53 (Al) showed a much higher Q_{st} value for CO_2 as shown in Table 13.

Pores functionalized with basic nitrogen-containing organic groups have been intensively studied for CO_2 adsorption properties.[90,91,95,118,125] The dispersion and electrostatic forces are typically responsible for the enhanced CO_2 adsorption. In some cases, acid–base type interactions between the lone-pair of nitrogen and CO_2 have been observed. To date, three major classes of nitrogen-functionalized metal–organic frameworks have been synthesized: heterocyclic derivatives (*i.e.* pyridine), aromatic amine derivatives (*i.e.* aniline), and alkylamine (*i.e.* ethylenediamine) bearing frameworks (Fig. 18). The commercial availability of aromatic amine containing linkers, especially 2-aminoterephthalic acid (NH_2-BDC), and the expected affinity of amino groups toward CO_2 have generated significant interest in aromatic amine functionalized frameworks. For example, $Ni_2(NH_2\text{-BDC})_2$(DABCO), Al(OH)(NH_2-BDC) (NH_2-MIL-53(Al)) and In(OH)(NH_2-BDC) have been shown to enhance CO_2 capture, when their low-pressure capacities are compared with that of the parent material.[89] Recently, it was proved that the aromatic amine of compound NH_2-MIL-53(Al) has a direct interaction with adsorbed CO_2 at low pressures.[218] However, the amine may not always be directly responsible for the enhanced adsorption. DFT calculations have shown that interactions between CO_2 and hydroxyl groups, that line the pore surfaces, were stronger than interactions between CO_2 and the amino functionalized material because of the increased acidity of the hydroxyl moieties. Amines are generally expected to enhance CO_2 adsorption in porous materials by acid–base chemistry, electrostatic forces, or enhanced dispersion forces. In the case of functionalization, the actual mechanism of binding, when fully elucidated, was shown to be quite different from those observed in non-functionalized frameworks.[70]

In order to mimic the chemisorptive interactions that are observed in aqueous amine scrubbers, more basic amine species need to be incorporated onto the pore surfaces of materials. W. Lu *et al*. used amine-grafted porous polymer networks.[51a] Under ultradilute conditions, the calculation using ideal adsorption solution theory showed their great potential for CO_2 capture application. The other strategy for

Table 13 Experimental Q_{st} values for CO_2 and CO_2 adsorption

		CO_2 adsorption		
MOFs	Q_{st} (kJ mol^{-1})	mg g^{-1}	Condition	Ref.
Mg-MOF-74	47	286.6	25 °C, 0.167 bar	217
Ni-MOF-74	41	206.5	25 °C, 0.167 bar	217
CO-MOF-74	37	170.6	25 °C, 0.167 bar	217
HKUST-1	12–35	43.4	25 °C, 0.167 bar	217
MIL-47	20–25	13.3	25 °C, 0.167 bar	217
MIL-53	20	96	30 °C, 5 bar	162
Amine-MIL-53	38.4	294	30 °C, 5 bar	162
IRMOF-3	16–20	8.2	25 °C, 0.167 bar	217
IRMOF-1	15	6.5	22 °C, 0.167 bar	217

controlling the pore size and creating desired functionalities in MOFs is the post-synthesis modification of pre-constructed, robust precursor MOFs.[51b] Because of direct-assembly strategies, certain functional groups may be hard to incorporate into MOFs, either because of instability under conditions for MOF synthesis or because of competitive reactions with intended framework components.[219] Examples of post-synthesis, amine-appended metal–organic frameworks (MOFs), such as mmen-Mg_2(dobpdc) have shown promising results to capture CO_2 from ultradilute gas streams.[219a] As illustrated in Fig. 18, alkylamine incorporation into the open metal sites of Cu-BTTri was found to be an effective method for post-synthetically modifying this metal–organic framework to enhance the CO_2 binding.[85,87] Farha *et al.* synthesized a series of cavity-modified MOFs by replacing coordinated solvents with several different pyridine ligands.[219b] Among them, a *p*-$(CF_3)NC_5H_4$-modified MOF showed considerable improvements in the CO_2–N_2 and CO_2–CH_4 selectivities compared to the unmodified parent MOF.[161] This was attributed to the highly polar $-CF_3$ functional groups as well as the constructed pores of the modified MOF (Fig. 19). This suggests that post-synthesis modification of MOFs by replacing coordinated solvent molecules with highly polar ligands may be a powerful method for generating new MOFs for CO_2 separation processes.

An important route to install the desired functionalities on the organic bridging units is the post-synthetic modification of the surface functional groups following the initial formation of the crystalline structure.[52,53] One advantage of such an approach is that functional groups that might interfere with the formation of the framework owing to their propensity to bind metal ions (such as amines, alcohols, and aldehydes) can be installed with well-known organic transformations once the framework scaffold has been formed, eliminating the need to develop precise reaction conditions to form the material directly. Such a procedure has been demonstrated on compounds such as IRMOF-3,[220] DMOF-1-NH_2,[221,222] UiO-66-Br,[223a] MIL-47(V)[223b] and MIL-101(Cr),[224] and the scope of reactions available is growing rapidly.

In addition to the size and shape (catenation) of the pores in MOFs, important factors that influence largely the separation performance of MOFs for a certain gas mixture, a suitable pore size that leads to strong confinement effects to induce large

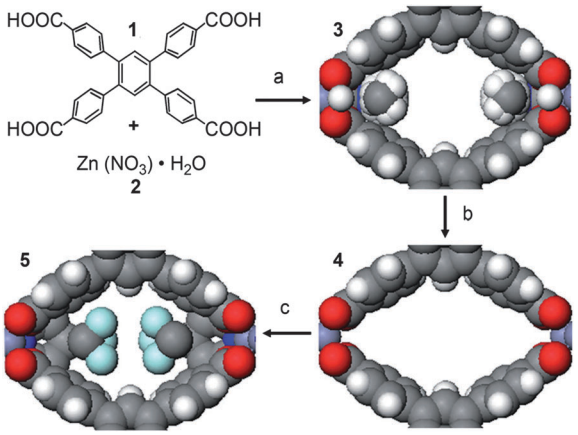

Fig. 19 An example of post-synthesis modification. First, the MOF is synthesized in DMF, and non-coordinated solvent molecules are removed by evacuation during heating at 100 °C to yield **3**, in which the coordinated DMF molecules remain. In step b, the material is heated at 150 °C to remove the coordinated DMF molecules and open metal sites in **4** are created. In step c, **4** is soaked in a solution of $CHCl_3$–4-(trifluoromethyl) pyridine, followed by evacuation during heating at 100 °C. Reproduced from ref. 161.

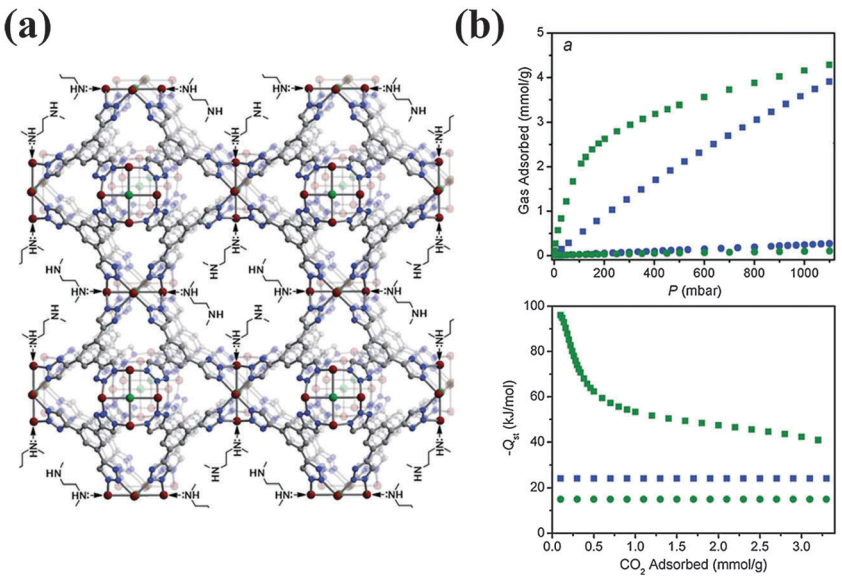

Fig. 18 (a) Functionalization of the metal–organic framework Cu-BTTri through binding *N,N′*-dimethylethylenediamine (mmen) to the open metal coordination sites; dark red, green, grey, and blue spheres represent Cu, Cl, C and N atoms, respectively. (b) (top) CO_2(■) and N_2(●) adsorption isotherms collected at 25 °C for Cu-BTTri (green symbols) and Cu-BTTri (blue symbols); (bottom) a plot of the isosteric heat of adsorption of CO_2(■) and N_2(●) in mmen-Cu-BTTri (green symbols) and Cu-BTTri (blue symbols). Reproduced from ref. 85.

differences in adsorbate–adsorbent interactions is crucial to create high selectivity. Greathouse *et al.* investigated the separation of noble gases in IRMOF-1, and found that when Xe is mixed with smaller atoms (Ar) the selectivity for Xe is larger than that in the mixture with larger atoms (Kr).[204] The optimization of MOFs for gas separation should involve the examination of the atomic properties of both feed gas and the substrate. The catenated structure in IRMOFs can be generated in different types of pores and thus induces larger differences in the adsorbate–IRMOF framework interactions between different components.[205] Similar results have been found for CO_2–N_2 and CH_4–N_2 mixtures in these MOFs, as well as for CO_2–CH_4 and both C_4 and C_5-alkane isomer mixtures in the catenated MOFs of IRMOF-13 and PCN-6 and their noncatenated counterparts, IRMOF-14 and PCN-60.[199,206] Moreover, the selectivity behaviour in catenated IRMOFs is more complicated, with a common trend in all the examined gas compositions: a rapid decrease of selectivity is observed at low pressures, which becomes more pronounced with increasing CH_4 or CO_2 concentration.[205] In addition, Gallo and Glossman-Mitnik also discussed the enhancement effect of the catenated structure on the selectivity by calculating the energetic interactions between the adsorbate and the framework.[207]

5.4 Extra framework cations

Incorporating a unique subset of ion-exchanged MOFs has received great attention, which contains charged frameworks and charge balancing extra-framework ions. Jiang and co-workers predicted, for the first time, the separation of CO_2–CH_4 in MOFs with extra-framework ions using molecular simulations.[199] Molecular dynamics and Grand Canonical Monte Carlo simulations (GCMC) indicated that the NO_3^- ions in *soc*-MOF essentially vibrate around their favourable location sites, which act as additional sites, particularly for quadrupolar CO_2 molecules, and thus substantially enhance the selectivity of CO_2 over CH_4. The relative selectivity of CO_2 over CH_4 increases from 22 to 36 at 27 °C as pressure rises from 0.0 to 5.0 MPa. From their simulation, it follows that the result can also be attributed to the strong interactions between CO_2 molecules and multiple binding sites in *soc*-MOF, and can be further promoted by the cooperative interactions of adsorbed CO_2 molecules. The effect of charges was examined by simulating the selectivity for a mixture in neutral framework structures by switching off the charges. For the CO_2–CH_4 mixture, the selectivity exhibited qualitative behaviour; with increasing pressure, the selectivity initially decreased due to the heterogeneous distribution of adsorption sites, and then increased due to the cooperative interactions between CO_2 molecules.

A computational method has been used by Mu *et al.* to study the effect of metal doping.[225] Their results have indicated the MOFs doped with alkali metals can greatly enhance the adsorption selectivity of the CO_2–CH_4 mixture (as shown in Fig. 20). The presence of alkali metal atoms contributed to the weak first ionization energies and low Lennard-Jones (LJ) potential parameters. The large length arising from the aromatic ring in the linkers of MOFs would enhance electrostatic interactions and weaken steric hindrance effects, and consequently improve the adsorption selectivity of CO_2 from the CO_2–CH_4 mixture.

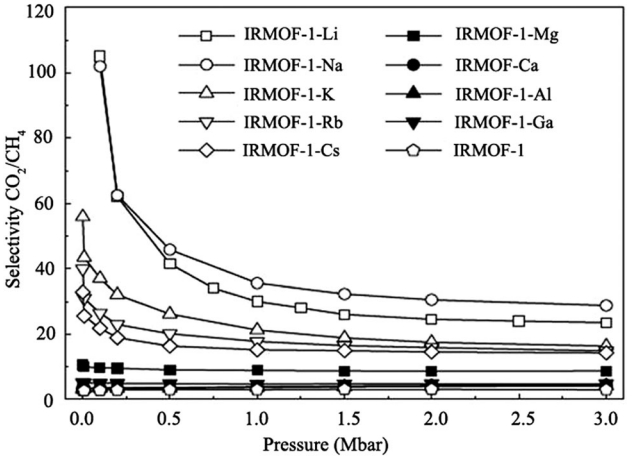

Fig. 20 Selectivity of CO_2 from a CO_2–CH_4 mixture with a gas composition of 10% CO_2 and 90% CH_4 at 25 °C. Reprinted from ref. 225, Copyright 2011, with permission from Elsevier.

Recently, incorporation of lithium ions into MOFs has attracted considerable interest because of the potential to obtain high Q_{st} values for H_2.[226,227] Mulfort *et al.* demonstrated two strategies for incorporating Li cations into MOFs by chemical reduction[149–151] with Li metal and exchanging hydroxyl protons in a MOF linker for Li cations.[228,229] Farha *et al.* showed that chemical reduction could enhance the CO_2–CH_4 selectivity in a diimide-based porous organic polymer (POP).[230] Later, Bae *et al.* have shown that Li cation incorporation into MOFs, by chemical reduction or cation exchange, significantly improves the CO_2–CH_4 selectivity.[121] Recently, a computational study predicted that *rho*-ZMOF, which contains an anionic framework and charge-balancing extra framework Na^+ ions, should display highly selective CO_2 adsorption over H_2, CH_4, and N_2.[231] These simulations demonstrate that the presence of extra framework ions is beneficial for separation of gas mixtures which have components with large differences in dipole and/or quadrupole moments. This suggests that the introduction of extra-framework ions is a useful method to enhance the electrostatic interactions between adsorbents and MOFs, which can lead to improved separation performance.

6. Future prospects for biogas upgrading using MOFs

In the current technology for biogas upgrading for application as high-quality fuel, sulphur (as H_2S) and ammonia (NH_3) contaminants are removed before the main separation of CO_2 from CH_4 as summarized in Tables 3 and 5 by using solvent scrubbers or solid adsorbents (pre-treatment process). However, based on a literature survey, MOFs have been slightly explored for this application to date. An example of H_2S and SO_2 gas separation was demonstrated on Zn(bchp) (H_2bcph = 2,2′-bis-(4-carboxyphenyl) hexafluoropropane).[232] The adsorption of H_2S

in MIL-53(Al, Cr, Fe), MIL-47, MIL-100(Cr), and MIL-101 also revealed that all of these MOFs are stable toward this corrosive gas and actually have high loading capacities and are easily regenerated, thus making them potential candidates for the purification of biogas.[233,234]

One crucial issue affecting the separation performance is moisture in gas mixtures. From systematic simulation studies in various neutral and ionic MOFs, Jiang *et al.* observed four different intriguing effects of H_2O on CO_2 capture.[231] It is perceived that the zinc-carboxylate based MOF-5 is water sensitive and begins to lose crystallinity upon exposure to small amounts of humidity.[138,235] Molecular dynamics simulations showed that the mechanism of hydrolysis for MOF-5 likely involves the direct attack of H_2O at the tetrahedral Zn^{2+} centers to displace bound BDC^{2-} ligands and destroy the framework structure.[236] One of the primary efforts to increase the water stability of metal–organic frameworks has been through the use of azolate-based linkers rather than the typical carboxylate linkers.[237–239] The azolate linkers can bind metals with a similar geometry to carboxylate ligands, but their greater basicity typically leads to stronger M–N bonds and greater thermal and chemical stability in the resulting framework. The stability of $Ni_3(BTP)_2$ (H_3BTP = 1,3,5-tris(1*H*-pyrazol-4-yl)benzene) is remarkable, this compound is stable in boiling water at pH 2–14 for at least 14 days.[239]

It is also instructive to examine structural changes in flexible MOFs that might occur upon adsorption.[240] The incorporation of flexibility to simulate structural changes would need a robust force field. An advantage of porous solid materials is the ability to modify their properties by impregnating or tethering active groups such as alkyl-amines onto their internal surfaces. The production of hybrid materials also holds great promise. For example, metal–organic frameworks could be closely integrated with hydrophobic polymers to produce block co-polymers which prohibit the permeation of water. Most recently, in order to improve the CO_2 separation performance of polymeric membranes, an amino-functionalized metal–organic framework, NH_2-MIL-53, was incorporated into polysulfone.[241] Presumably due to the hydrogen bond interactions between the amine functionalities within the metal–organic framework and the sulfone groups of the polymer, high NH_2-MIL-53 loadings of up to 40 wt% were achieved. However, the best CO_2–CH_4 separation performance was observed in 25 wt% NH_2-MIL-53 loaded membranes. Composite materials of MOFs (MOF-5, HKUST-1 or MIL-100(Fe)) with graphitic compounds (graphite or graphite oxide (GO)) were tested for the removal of NH_3, H_2S and NO_2 under ambient conditions.[242] Characterization of the composite materials indicated that strong chemical bonds exist between the MOF and GO as a result of the coordination between the GO oxygen and the MOFs' metallic centers, which enhances the physical adsorption capacity of the toxic gases. In particular, depending on the structure of the MOF, such interactions can induce the formation of a new pore space in the interface between the carbon layers and the MOF units.

As mentioned above, composites are multicomponent materials comprising multiple different (nongaseous) phase domains in which at least one type of phase domain is a continuous phase.[243] They are often used in industrial processes, since the composites combine the properties of the phases and tuning of the properties is possible. In addition, handling of the composites is often easier compared to the crystalline MOFs. A combination of outstanding properties of each material, such as high CO_2 capture of zeolite, hydrophobic nature of some MOFs and metal base oxides (increasing the interactions between carbon dioxide and the adsorbent), should generate high performing adsorbents.

The combination of material synthesis, characterization, and computation requires a significant critical mass of expertise of a scope only afforded through extensive scientific collaborations. As a burgeoning field, research activities in MOFs are rather hectic. It is evident that the progress and achievement of almost all of these adsorbents rely heavily on the development of adsorbent materials. The majority challenges of the proposed adsorbents that arise in the development of these materials and techniques lie in being able to transfer the technology from the lab to commercial level that can be achieved by maximizing efficiency and minimizing costs. Thus, the discovery of new MOF adsorbent materials with high separation ability becomes one of the biggest challenges. This review article has sought to highlight the challenges of ideal MOF material adsorbents, which have the greatest likelihood of upgrading biogas, *via* CO_2 capture. The ideal MOF adsorbent should be exhibiting extraordinarily high CO_2 uptake and selectivity at near-ambient pressures. Furthermore, the ideal MOF adsorbent should be highly stable, particularly in the presence of small amounts of moisture, and should be easily regenerated for long-term usage. The selection of the optimum adsorbent for CO_2 capture will depend on the process used, the adsorbent performance, adsorbent lifetime, and adsorbent cost, among other factors. Although in the scientific literature authors most often focus on adsorbent capacity as a design metric, in this work we highlighted and reviewed the multitude of technical parameters that need to be considered for any adsorbent that will be utilized in biogas *via* carbon dioxide capture.

7. Conclusions and remarks

Metal–organic frameworks are new adsorbents used for storage of several gases and separation processes. They have more advanced properties than other solid adsorbents such as high crystallinity, robustness, high gas storage ability, high regenerability *etc.* They are easily tuneable by virtue of the fact that they are self-assembled from metal salts and nearly infinitely variable organic ligands, which can be used to introduce functional groups to a pore surface, precisely control pore metrics, and impart the material with a structure flexibility that is unprecedented in other types of materials. MOF adsorbents can be successfully applied for carbon dioxide–methane (CO_2–CH_4) separation for biogas upgrading. Their potential may boost new development in adsorption technology for gas molecules. Successfully applicable MOF adsorbents should expand the application of biogas utilization as an environmentally friendly

and sustainable fuel. In addition to affecting the biogas upgrading, the impurity components (NH_3, H_2S and H_2O) will also inevitably require consideration in terms of the long-term stability of the adsorptive materials, as well as the energy requirements for regeneration.

The performance of the materials should be evaluated in the context of engineering process models that take performance parameters, such as the working capacity and selectivity, as input to allow optimized working conditions to be developed for each adsorbent. Despite their potential aspects, no industrial application in the biogas upgrading is yet available using MOF compounds. There is still much research required to successfully develop MOFs for adsorption technology. However, a strong link between materials science and process engineering can contribute to develop this technology faster. The challenge that arises in the development of these materials and techniques lies in being able to transfer the technology from the lab to the harsh industrial conditions where the improvement will be subjected to maximizing efficiency and minimizing costs.

Abbreviations

abtc	3,3′,5,5′-Azobenzenetetracarboxylate
ACMP	Acetylene-mediated conjugated microporous polymers
ADA	Adamantanediacetate
adc	4,4′-Azobenzenedicarboxylate
ade	Adenine
almeIm	4-Methylimidazole-5-carbaldehyde
atz	3-Amino-1,2,4-triazole
BBC	4,4′,4″-(Benzene-1,3,5-triyl-tris(benzene-4,1-diyl))-tribenzoate
bbIm	5-Bromobenzimidazole
bbs	Dianion of 4,4′-bibenzoic acid-2,2′-sulfone
bcphfp	2,2′-Bis(4-carboxyphenyl)hexafluoropropane
BDC	1,4-Benzenedicarboxylate
Bdcppi	*N*,*N*′-Bis(3,5-dicarboxyphenyl)pyromellitic diimide
bdi	5,50-(Buta-1,3-diyne-1,4-diyl)diisophthalate
BDoborDC	1,4-Bis(1,12-dicarbonyl-*closo*-dodecaborane)-benzene
bIm	Benzimidazole
BME-bdc	2,5-Bis(2-methoxyethoxy)benzene-1,4-dicarboxylate
BPDC	Biphenyl-4,40-dicarboxylate
bpe	1,2-Bis(4-pyridyl)ethane
bpee	1,2-Bis(4-pyridyl)ethylene
bpetha	1,2-Bis(4-pyridyl)ethane
BPnDC	Benzophenone-4,4′-dicarboxylic acid
bpdc	Biphenyl-4,4′-dicarboxylate
bpp	1,3-Bis(4-pyridyl)propane
bpta	3,6-Di(4-pyridyl)-1,2,4,5-tetrazine
bptb	2,2′-Biphenol-3,3′,5,5′-tetrakis(4-benzoate)
bptc	3,3′,5,5′-Biphenyltetracarboxylic acid
bpy	4,4′-Bipyridine
bpydc	2,2′-Bipyridine-5,5′-dicarboxylate
BTB	4,4′,4″-Benzene-1,3,5-triyl-tribenzoate
BTC, btc	1,3,5-Benzenetriscarboxylate
btdc	2,2′-Bithiophene-5,5′-dicarboxylate
BTT	4,4′,4″-(Benzene-1,3,5-triyl-tris(ethyne-2,1-diyl))-tribenzoate
btei	5,5′,5″-Benzene-1,3,5-triyl-tris(1-ethynyl-2-isophthalate)
BTetB	4,4′,4″,4‴-Benzene-1,2,4,5-tetrayltetrabenzoic acid
BTP	1,3,5-Tris(1*H*-pyrazol-4-yl)benzene
bttb	4,4′,4″,4‴-Benzene-1,2,4,5-tetrayl-tetrabenzoate
cbIm	5-Chlorobenzimidazole
CDC	1,12-Dihydroxydicarbonyl-1,12-dicarba-closododecaborane
CEbnbpy	(*R*)-6,6′-Dichloro-2,2′-diethoxy-1,1′-binaphthyl-4,4′bipyridine
cis-chdc	1,4-Cyclohexanedicarboxylate
CNBPDC	2,2′-Dicyano-4,4′-biphenyldicarboxylic acid
CNC	4-Carboxycinnamate
cnIm	4-Cyanoimidazole
CNT	Carbon nanotubes
CPI	5-(4-Carboxy-phenoxy)isophthalate
CPOM	[(4-Carboxyphenyl)oxamethyl]methanoate
cyamIm	4-Aminoimidazole-5-carbonitrile
cyclam	1,4,8,11-Tetraazacyclotetradecane
dabco	Triethylenediamine (1,4-diazabicyclo[2.2.2]octane)
DBM	Dibenzoylmethanato
DBS	4,4′-Dibenzoate-2,20-sulfone
dcIm	4,5-Dichloroimidazole
dhbc	2,5-Dihydroxybenzoate
dhbpc	4,4′-Dihydroxybiphenyl-3-carboxylate
DOT	Dihydroxyterephthalic acid
DCTP	3,3″-Dicarboxy-1,1′:4′,1″-terphenyl
dImb	1,4-Di(1*H*-imidazol-4-yl)benzene
diPyNI	*N*,*N*′-Di-(4-pyridyl)-1,4,5,8-naphthalenetetracarboxydiimide
DMA	*N*,*N*′-Dimethylacetamide
dobdc	2,5-Dioxido-1,4-benzenedicarboxylate
doborDC	1,12-Dihydroxy-carbonyl-1,12-dicarba-closododecaborane
dpa	1,1′-Biphenyl-2,2′-dicarboxylate
dpe	1,2-Di(4-pyridyl)ethylene
DPG	*meso*-1,2-Bis(4-pyridyl)-1,2-ethanediol
dpni	*N*,*N*′-Di-(4-pyridyl)-1,4,5,8-naphthalenetetracarboxydiimide
dpntcd	*N*,*N*-Di(4-pyridyl)-1,4,5,8-naphthalenetetracarboxydiimide
DPT	3,6-Di-4-pyridyl-1,2,4,5-tetrazine
EBTC	1,1′-Ethynebenzene-3,3′,5,5′-tetracarboxylate
eIm	2-Ethylimidazole
ELM	Elastic layer-structured MOF
etz	2,5-Diethyl-1,2,4-triazole
FMA	Fumarate
F-pymo	5-Fluoropyrimidin-2-olate
Gly-Ala	Glycylalanine

hymeIm	4-Hydroxymethyl-5-methylimidazole
H_4abtc	1,1′-Azobenzene-3,3′,5,5′-tetracarboxylic acid
H_4bdi	5,5′-(Buta-1,3-diyne-1,4-diyl)diisophthalic acid
H_3BPT	Biphenyl-3,4′,5-tricarboxylate
H_2bpydc	2,2′-Bipyridine-5,5′-dicarboxylic acid
H_2BPDC	4,4′-Biphenyldicarboxylic acid
H_3BTTri	1,3,5-Tri(1*H*-1,2,3-triazol-4-yl)benzene, 4′-*tert*-butyl-biphenyl-3,5-dicarboxylate
H_4DHBP	1,4-Dihydroxy-2,5-benzenediphosphonic acid
H_4dobdc	2,5-Dioxido-1,4-benzenedicarboxylate
H_2fipbb	4,4′-(Hexafluoroisopropylidene)-bis(benzoic acid)
H_3idc	4,5-Imidazoledicarboxylic acid
H_4MTB	Methanetetrabenzoic acid
H_2obb	4,4′-Oxybis(benzoic acid)
Hoxonic	4,6-Dihydroxy-1,2,3-triazine-2-carboxylic acid
H_2ppt	3-(2-Phenol)-5-(4-pyridyl)-1,2,4-triazole
H_3pzdc	3,5-Pyrazoledicarboxylic acid
H_2tcpbda	*N,N,N′,N′*-Tetrakis(4-carboxyphenyl)-biphenyl-4,4′-diamine
IBPDC	Dimethyl-2,2′-diiodo-4,4′-biphenyldicarboxylate
IDC	2-Methylimidazolate-4-amide-5-imidate
Im	Imidazole
L1, L2	Ethyl- and butyl-bridged Ni_2 macrocyclic complexes
MAF	Metal azolate framework
MAMS	Mesh-adjustable molecular sieves
mbIm	5-Methylbenzimidazole
mdpt24	3-(3-Methyl-2-pyridyl)-5-(4-pyridyl)-1,2,4-triazolate
Me_4bpz	3,3′,5,5′-Tetramethyl-4,40-bis(pyrazolate)
mIm	2-Methylimidazole
m-TATB	3,3′,3″-*s*-Triazine-2,4,6-triyltribenzoate
mtb	Methanetetrabenzoate
nbIm	5-Nitrobenzimidazole
NDC	2,6-Naphthalenedicarboxylate
nIm	2-Nitroimidazole
NH_2bdc	2-Amino-1,4-benzenedicarboxylate
NTC	Naphthalene-1,4,5,8-tetracarboxylate
ntei	5,5′,5″-(4,4′,4″-Nitrilotris(benzene-4,1-diyl)-tris(ethyne-2,1-diyl))triisophthalate
pba	4-(Pyridin-4-yl)benzoate
pbmp	*N,N′*-Piperazinebismethylenephosphonate
p-CDC	1,12-Dihydroxycarbonyl-1,12-dicarba-*closo*-dodecaborane
p-cdc^{2-}	Deprotonated form of 1,12-dihydroxydicarbonyl-1,12-dicarba-*closo*-dodecaborane
pdc	3,5-Pyridinedicarboxylate
PDC	Pyrenedicarboxylic acid
phen	1,10-Phenanthroline
pmc	Pyrimidine-5-carboxylate
pmdc	Pyrimidine-4,6-dicarboxylate
py	Pyridine
pydc	3,5-Pyridinedicarboxylate
pymo	Pyrimidinolate
pyrdc	Pyridine-2,3-dicarboxylate
pyz	Pyrazine
pzdc	2,3-Pyrazinedicarboxylate
SCA	Sulfonatocalix[4]arene
TATB	4,4′,4′-*s*-Triazine-2,4,6-triyl-tribenzoate
TBA	Tetrabutylammonium
TCEPEB	1,3,5-Tris[(1,3-carboxylic acid-5-(4-ethynyl)phenyl)-ethynyl]benzene
TCM	Tetrakis[4-(carboxyphenyl)-oxamethyl]methane
TCMO	Tetrakis[4-(carboxyphenyl)-oxamethyl]methanoate
TCPB	1,2,4,5-Tetrakis(4-carboxyphenyl)benzene
TCPBDA	*N,N,N′,N′*-Tetrakis(4-carboxyphenyl)-biphenyl-4,-4′-diamine
TDCPTM	4,4′,4″,4‴-Tetrakis[3,5-di(carboxylate)-1-phenyl]-tetraphenyl methane
TEA	Tetraethylammonium
TED	Triethylenediamine
tImb	1,3,5-Tris(1*H*-imidazol-4-yl)benzene
TMA	Tetramethylammonium
TPBTM	*N,N′,N″*-Tris(isophthalyl)-1,3,5-benzenetricarboxamide

Acknowledgements

The authors would like to express their deep appreciation to State Key Lab of Advanced Technology for Materials Synthesis and Processing for financial support (Wuhan University of Technology, 2013-KF-5). F.V. acknowledges the Chinese Central Government for an ''Expert of the State'' position in the program of ''Thousand talents''.

References

1 S. A. Rackley, *Carbon Capture and Storage*, Elsevier, 2010.
2 B. Metz, O. Davidson, H. de Coninck, M. Loos and L. Meyer, *Intergovernmental Panel on Climate Change. Special Report on Carbon Dioxide Capture and Storage*, Cambridge University Press, Cambridge, 2005.
3 A. P. Sokolov, P. H. Stone, C. E. Forest, R. G. Prinn, M. C. Sarofim, M. Webster, S. Paltsev, C. A. Schlosser, D. Kicklighter, S. Dutkiewicz, J. M. Reilly, C. Wang, B. Felzer and H. D. Jacoby, *J. Clim.*, 2009, **22**, 5175–5204.
4 Key GHG Data, United Nations Framework Convention on Climate Change, Bonn, Germany, 2005.
5 Helmut Kaiser Consultancy, Clean Energy and Renewable Energy Market Worldwide 2007-2010-2015: http://www.hkc22.com/biogas.html.
6 National Non-Food Crops Centre. ''NNFCC Renewable Fuels and Energy Factsheet: Anaerobic Digestion'', 2011.
7 L. A. Kristensen, BIOGAS IN SOCIETY, A Success Story from IEA BIOENERGY TASK 37 ''Energy from Biogas'', 2013.
8 K. S. Knaebel and H. E. Reinhold, *Adsorption*, 2003, **9**, 87–97.
9 M. Hagen, E. Polman, J. K. Jensen, A. Myken, O. Jönsson, A. Dahl, Adding gas from biomass to the gas grid. Report SGC 118, Swedish Gas Centre, 2001.

10 Y. S. Bae, K. L. Mulfort, H. Frost, P. Ryan, S. Punnathanam, L. J. Broadbelt, J. T. Hupp and R. Q. Snurr, *Langmuir*, 2008, **24**, 8592–8598.
11 S. K. Ritter, *Chem. Eng. News*, 2007, **85**, 7.
12 B. Kumar, J. M. Smieja and C. P. Kubiak, *J. Phys. Chem. C*, 2010, **114**, 14220–14223.
13 A. Petersson, A. Wellinger, Biogas upgrading technologies-developments and innovations, IEA Bioenergy, Task37-Energy from biogas and landfill gas, 2009.
14 Matt McGrath, Environment Correspondent, BBC–the original article: http://www.bbc.co.uk/news/science-environment-21320666.
15 S. Sridhar, B. Smitha and T. M. Aminabhavi, *Sep. Purif. Rev.*, 2007, **36**, 113–174.
16 R. T. Yang, *Gas Separation by Adsorption Processes*, Imperial College Press, London, 1997.
17 R. Bredesen and T. A. Peters, in *Membrane Technology*, ed. K.-V. Peinemann and S. P. Nunes, Wiley-VCH, Weinheim, 2008, vol. 2.
18 (*a*) S. Sircar, Pressure Swing Adsorption, *Ind. Eng. Chem. Res.*, 2002, **41**, 1389–1392; (*b*) J. P. Sculley, W. M. Verdegaal, W. Lu, M. Wriedt and H.-C. Zhou, *Adv. Mater.*, 2013, **25**, 3957–3961.
19 R. T. Yang, *Gas Separation by Adsorption Processes*, Butterworths, Boston, 1987.
20 J. Stçcker, M. Whysall, G. Q. Miller, 30 years of PSA technology for hydrogen purification, UOP, 1998.
21 D. Aaron and C. Tsouris, *Sep. Sci. Technol.*, 2005, **40**, 321–348.
22 M. Hagen, E. Polman, J.K. Jensen, A. Myken, O. Jönsson, A. Dahl, Report SGC 118, Swedish Gas Centre: Scheelegatan, Sweden, 2001.
23 A. L. Chaffee, G. P. Knowles, Z. Liang, J. Zhany, P. Xiao and P. A. Webley, *Int. J. Greenhouse Gas Control*, 2007, **1**, 11–18.
24 E. H. M. Dirkse, Technologies for biogas upgrading. Theme sessions 1 Green Gas: from production to user. Conference sustainable mobility; energy valley, Leeuwarden. November 2006.
25 D. M. D'Alessandro, B. Smit and J. R. Long, *Angew. Chem.*, 2010, **122**, 6194–6219.
26 S. Cavenati, C. A. Grande and A. E. Rodrigues, *Energy Fuels*, 2006, **20**, 2648–2659.
27 S. Cavenati, C. A. Grande and A. E. Rodrigues, *J. Chem. Eng. Data*, 2004, **49**, 1095–1101.
28 P. Y. Li and F. H. Tezel, *Microporous Mesoporous Mater.*, 2007, **98**, 94–101.
29 J. M. Leyssale, G. K. Papadopoulos and D. N. Theodorou, *J. Phys. Chem. B*, 2006, **110**, 22742–22753.
30 R. Babarao, Z. Q. Hu, J. W. Jiang, S. Chempath and S. I. Sandler, *Langmuir*, 2007, **23**, 659–666.
31 M. B. Kim, Y. S. Bae, D. K. Choi and C. H. Lee, *Ind. Eng. Chem. Res.*, 2006, **45**, 5050–5058.
32 A. Kapoor and R. T. Yang, *Chem. Eng. Sci.*, 1989, **44**, 1723–1734.
33 X. Peng, W. C. Wang, R. S. Xue and Z. M. Shen, *AIChE J.*, 2006, **52**, 994–1003.
34 V. Goetz, O. Pupier and A. Guillot, *Adsorption*, 2006, **12**, 55–63.
35 S. Cavenati, C. A. Grande and A. E. Rodrigues, *Energy Fuels*, 2005, **19**, 2545–2555.
36 R. Q. Snurr, J. T. Hupp and S. T. Nguyen, *AIChE J.*, 2004, **50**, 1090–1095.
37 J. L. C. Rowsell and O. M. Yaghi, *Angew. Chem., Int. Ed.*, 2005, **44**, 4670–4679.
38 U. Mueller, M. Schubert, F. Teich, H. Puetter, K. Schierle-Arndt and J. Pastre, *J. Mater. Chem.*, 2006, **16**, 626–636.
39 S. Surble, F. Millange, C. Serre, T. Düren, M. Latroche, S. Bourrelly, P. L. Llewellyn and G. Ferey, *J. Am. Chem. Soc.*, 2006, **128**, 1488–1490.
40 J. H. Martin, Biological and Agriculture Engineering, MPhil thesis, North Carolina State University, 2008.
41 S. Natarajan and S. Mandal, *Angew. Chem., Int. Ed.*, 2008, **120**, 4876–4907.
42 D. J. Tranchemontagne, Z. Ni, M. O'Keeffe and O. M. Yaghi, *Angew. Chem., Int. Ed.*, 2008, **120**, 5214–5225.
43 M. O'Keeffe, M. A. Peskov, S. J. Ramsden and O. M. Yaghi, *Acc. Chem. Res.*, 2008, **41**, 1782–1789.
44 J.-R. Li, Y. Ma, M. C. McCarthy, J. Sculley, J. H.-K. Jeongb, P. B. Balbuena and H.-C. Zhou, *Coord. Chem. Rev.*, 2011, **255**, 1791–1823.
45 D. Q. Yuan, D. Zhao, D. F. Sun and H. C. Zhou, *Angew. Chem., Int. Ed.*, 2010, **49**, 5357–5361.
46 J. Klinowski, F. A. Almeida Paz, P. Silva and J. Rocha, *Dalton Trans.*, 2011, **40**, 321–330.
47 O. K. Farha and J. T. Hupp, *Acc. Chem. Res.*, 2010, **43**, 1166–1175.
48 O. K. Farha, I. Eryazici, N. C. Jeong, B. G. Hauser, C. E. Wilmer, A. A. Sarjeant, R. Q. Snurr, S. T. Nguyen, A. Ö. Yazaydn and J. T. Hupp, *J. Am. Chem. Soc.*, 2012, **134**, 15016–15021.
49 H. Furukawa, N. Ko, Y. B. Go, N. Aratani, S. B. Choi, E. Choi, A. O. Yazaydin, R. Q. Snurr, M. O'Keefe, J. Kim and O. M. Yaghi, *Science*, 2010, **329**, 424–428.
50 J. L. C. Rowsell and O. M. Yaghi, *J. Am. Chem. Soc.*, 2006, **128**, 1304–1315.
51 (*a*) W. Lu, J. P. Sculley, D. Yuan, R. Krishna and H.-C. Zhou, *J. Phys. Chem. C*, 2013, **117**, 4057–4061; (*b*) Z. Q. Wang and S. M. Cohen, *Chem. Soc. Rev.*, 2009, **38**, 1315–1329.
52 K. K. Tanabe and S. M. Cohen, *Chem. Soc. Rev.*, 2011, **40**, 498–519.
53 A. U. Czaja, N. Trukhan and U. Müller, *Chem. Soc. Rev.*, 2009, **38**, 1284–1293.
54 M. Eddaoudi, J. Kim, N. Rosi, D. Vodak, J. Wachter, M. O'Keeffe and O. M. Yaghi, *Science*, 2002, **295**, 469–472.
55 H. Furukawa, N. Ko, Y. B. Go, N. Aratani, S. B. Choi, E. Choi, A. O. Yazaydin, R. Q. Snurr, M. O'Keeffe, J. Kim and O. M. Yaghi, *Science*, 2010, **329**, 424–428.
56 X. S. Wang, S. Q. Ma, P. M. Forster, D. Q. Yuan, J. Eckert, J. J. Lopez, B. J. Murphy, J. B. Parise and H. C. Zhou, *Angew. Chem., Int. Ed.*, 2008, **47**, 7263–7266.
57 U.S.E.I. Administration, International Energy Annual, 2008.

58 J.-R. Li, R. J. Kuppler and H.-C. Zhou, *Chem. Soc. Rev.*, 2009, **38**, 1477–1504.
59 M. Kurmoo, *Chem. Soc. Rev.*, 2009, **38**, 1353–1379.
60 J. Y. Lee, O. K. Farha, J. Roberts, K. A. Scheidt, S. T. Nguyen and J. T. Hupp, *Chem. Soc. Rev.*, 2009, **38**, 1450–1459.
61 G. K. H. Shimizu, R. Vaidhyanathan and J. M. Taylor, *Chem. Soc. Rev.*, 2009, **38**, 1430.
62 S. Q. Ma and H. C. Zhou, *Chem. Commun.*, 2010, **46**, 44–53.
63 S. Choi, J. H. Drese and C. W. Jones, *ChemSusChem*, 2009, **2**, 796–854.
64 D. M. D'Alessandro, B. Smit and J. R. Long, *Angew. Chem., Int. Ed.*, 2010, **49**, 6058–6082.
65 H. Hayashi, A. P. Côté, H. Furukawa, M. O'Keeffe and O. M. Yaghi, *Nat. Mater.*, 2007, **6**, 501–506.
66 Y. L. Liu, V. C. Kravtsov, R. Larsen and M. Eddaoudi, *Chem. Commun.*, 2006, 1488–1490.
67 A. P. Cote, A. I. Benin, N. W. Ockwig, M. O'Keeffe, A. J. Matzger and O. M. Yaghi, *Science*, 2005, **310**, 1166–1170.
68 O. K. Farha, A. M. Spokoyny, B. G. Hauser, Y.-S. Bae, S. E. Brown, R. Q. Snurr, C. A. Mirkin and J. T. Hupp, *Chem. Mater.*, 2009, **21**, 3033–3035.
69 Electric Power Research Institute, *Program on Technology Innovation: Post-combustion CO_2 Capture Technology Development,* Electric Power Research Institute, Palo Alto, 2008.
70 A. R. Millward and O. M. Yaghi, *J. Am. Chem. Soc.*, 2005, **127**, 17998–17999.
71 K. Sumida, D. L. Rogow, J. A. Mason, T. M. McDonald, E. D. Bloch, Z. R. Herm, T.-H. Bae and J. R. Long, *Chem. Rev.*, 2012, **112**, 724–781.
72 (*a*) J.-R. Li, J. Sculley and H.-C. Zhou, *Chem. Rev.*, 2012, **112**, 869–932; (*b*) J. Liu, P. K. Thallapally, B. P. McGrail, D. R. Brown and J. Liua, *Chem. Soc. Rev.*, 2012, **41**, 2308–2322.
73 Z. Bao, L. Yu, Q. Ren, X. Lu and S. Deng, *J. Colloid Interface Sci.*, 2011, **353**, 549–556.
74 A. Ö. Yazaydin, R. Q. Snurr, T.-H. Park, K. Koh, J. Liu, M. D. LeVan, A. I. Benin, P. Jakubczak, M. Lanuza, D. B. Galloway, J. L. Low and R. R. Willis, *J. Am. Chem. Soc.*, 2009, **131**, 18198–18199.
75 J. A. Mason, K. Sumida, Z. R. Herm, R. Krishna and J. R. Long, *Energy Environ. Sci.*, 2011, **4**, 3030–3040.
76 D. Britt, H. Furukawa, B. Wang, T. G. Glover and O. M. Yaghi, *Proc. Natl. Acad. Sci. U. S. A.*, 2009, **106**, 20637–20640.
77 S. R. Caskey, A. G. Wong-Foy and A. J. Matzger, *J. Am. Chem. Soc.*, 2008, **130**, 10870–10871.
78 A. Ö. Yazaydin, A. I. Benin, S. A. Faheem, P. Jakubczak, J. J. Low, R. R. Willis and R. Q. Snurr, *Chem. Mater.*, 2009, **21**, 1425–1430.
79 J. Liu, Y. Wang, A. I. Benin, P. Jakubczak, R. R. Willis and M. D. LeVan, *Langmuir*, 2010, **26**, 14301–14307.
80 P. D. C. Dietzel, R. E. Johnsen, H. Fjellvag, S. Bordiga, E. Groppo, S. Chavan and R. Blom, *Chem. Commun.*, 2008, 5125–5127.
81 P. Aprea, D. Caputo, N. Gargiulo, F. Iucolano and F. Pepe, *J. Chem. Eng. Data*, 2010, **55**, 3655–3661.
82 P. Chowdhury, C. Bikkina, D. Meister, F. Dreisbach and S. Gumma, *Microporous Mesoporous Mater.*, 2009, **117**, 406–413.
83 D. Farrusseng, C. Daniel, C. Gaudillere, U. Ravon, Y. Schuurman, C. Mirodatos, D. Dubbeldam, H. Frost and R. Q. Snurr, *Langmuir*, 2009, **25**, 7383–7388.
84 J. Kim, S.-T. Yang, S. B. Choi, J. Sim, J. Kim and W.-S. Ahn, *J. Mater. Chem.*, 2011, **21**, 3070–3076.
85 T. M. McDonald, D. M. D'Alessandro, R. Krishna and J. R. Long, *Chem. Sci.*, 2011, **2**, 2022–2028.
86 J. An, S. J. Geib and N. L. Rosi, *J. Am. Chem. Soc.*, 2010, **132**, 38–39.
87 A. Demessence, D. M. D'Alessandro, M. L. Foo and J. R. Long, *J. Am. Chem. Soc.*, 2009, **131**, 8784–8786.
88 R. Vaidhyanathan, S. S. Iremonger, K. W. Dawson and G. K. H. Shimizu, *Chem. Commun.*, 2009, 5230–5233.
89 B. Arstad, H. Fjellvåg, K. O. Kongshaug, O. Swang and R. Blom, *Adsorption*, 2008, **14**, 755–762.
90 T. K. Prasad, D. H. Hong and M. P. Suh, *Chem.–Eur. J.*, 2010, **16**, 14043–14050.
91 K. Sumida, S. Horike, S. S. Kaye, Z. R. Herm, W. L. Queen, C. M. Brown, F. Grandjean, G. J. Long, A. Dailly and J. R. Long, *Chem. Sci.*, 2010, **1**, 184–191.
92 H. Kanoh, A. Kondo, H. Noguchi, H. Kajiro, A. Tohdoh, Y. Hattori, W.-C. Xu, M. Inoue, T. Sugiura, K. Morita, H. Tanaka, T. Ohba and K. Kaneko, *J. Colloid Interface Sci.*, 2009, **334**, 1–7.
93 E. D. Bloch, D. Britt, C. Lee, C. J. Doonan, F. J. Uribe-Romo, H. Furukawa, J. R. Long and O. M. Yaghi, *J. Am. Chem. Soc.*, 2010, **132**, 14382–14384.
94 C. Tan, S. Yang, N. R. Champness, X. Lin, A. J. Blake, W. Lewis and M. Schröder, *Chem. Commun.*, 2011, **47**, 4487–4489.
95 S.-S. Chen, M. Chen, S. Takamizawa, P. Wang, G.-C. Lv and W.-Y. Sun, *Chem. Commun.*, 2011, **47**, 4902–4904.
96 T. K. Kim and M. P. Suh, *Chem. Commun.*, 2011, **47**, 4258.
97 J. A. R. Navarro, E. Barea, J. M. Salas, N. Masciocchi, S. Galli, A. Sironi, C. O. Ania and J. B. Parra, *J. Mater. Chem.*, 2007, **17**, 1939–1946.
98 P. Rallapalli, K. P. Prasanth, D. Patil, R. S. Somani, R. V. Jasra and H. C. Bajaj, *J. Porous Mater.*, 2011, **18**, 205–210.
99 S. R. Miller, G. M. Pearce, P. A. Wright, F. Bonino, S. Chavan, S. Bordiga, I. Margiolaki, N. Guillou, G. Ferey, S. Bourrelly and P. L. Llewellyn, *J. Am. Chem. Soc.*, 2008, **130**, 15967–15981.
100 K. C. Stylianou, J. E. Warren, S. Y. Chong, J. Rabone, J. Basca, D. Bradshaw and M. J. Rosseinsky, *Chem. Commun.*, 2011, **47**, 3389–3391.
101 Z. Chen, S. Xiang, H. D. Arman, P. Li, S. Tidrow, D. Zhao and B. Chen, *Eur. J. Inorg. Chem.*, 2010, 3745–3749.
102 P. D. Southon, L. Liu, E. A. Fellows, D. J. Price, G. J. Halder, K. W. Chapman, B. Moubaraki, K. S. Murray, J.-F. Létard and C. J. Kepert, *J. Am. Chem. Soc.*, 2009, **131**, 10998–11009.
103 R. Banerjee, H. Furukawa, D. Britt, C. Knobler, M. O'Keefe and O. M. Yaghi, *J. Am. Chem. Soc.*, 2009, **131**, 3875–3876.

104 W. Morris, B. Leung, H. Furukawa, O. K. Yaghi, N. He, H. Hayashi, Y. Houndonougbo, M. Asta, B. B. Laird and O. M. Yaghi, *J. Am. Chem. Soc.*, 2010, **132**, 11006–11008.
105 F. Debatin, A. Thomas, A. Kelling, N. Hedin, Z. Bacsik, I. Senkovska, S. Kaskel, M. Junginger, H. Muller, U. Schilde, C. Jager, A. Friedrich and H.-J. Holdt, *Angew. Chem., Int. Ed.*, 2010, **49**, 1258–1262.
106 Z. X. Zhao, Z. Li and Y. S. Lin, *Ind. Eng. Chem. Res.*, 2009, **48**, 10015–10020.
107 D. Saha, Z. Bao, F. Jia and S. Deng, *Environ. Sci. Technol.*, 2010, **44**, 1820–1826.
108 C.-M. Lu, J. Liu, K. Xiao and A. T. Harris, *Chem. Eng. J.*, 2010, **156**, 465–470.
109 H. X. Deng, C. J. Doonan, H. Furukawa, R. B. Ferriera, J. Towne, C. B. Knobler, B. Wang and O. M. Yaghi, *Science*, 2010, **327**, 846–850.
110 P. L. Llewellyn, S. Bourrelly, C. Serre, Y. Filinchuk and G. Férey, *Angew. Chem., Int. Ed.*, 2006, **45**, 7751–7754.
111 Z. Chen, X. Liu, C. Zhang, Z. Zhang and F. Liang, *Dalton Trans.*, 2011, **40**, 1911–1918.
112 Z. Chen, S. Xiang, D. Zhao and B. Chen, *Cryst. Growth Des.*, 2009, **9**, 5293–5296.
113 Z. Zhang, S. Xiang, X. Rao, Q. Zheng, F. R. Fronczek, G. Qian and B. Chen, *Chem. Commun.*, 2010, **46**, 7205–7207.
114 G. Beobide, W.-G. Wang, O. Castillo, A. Luque, P. Román, G. Tagliabue, S. Galli and J. A. R. Navarro, *Inorg. Chem.*, 2008, **47**, 5267–5277.
115 J. A. R. Navarro, E. Barea, J. M. Salas, N. Masciocchi, S. Galli, A. Sironi, C. O. Ania and J. B. Parra, *Inorg. Chem.*, 2006, **45**, 2397–2399.
116 R. Banerjee, A. Phan, B. Wang, C. Knobler, H. Furukawa, M. O'Keefe and O. M. Yaghi, *Science*, 2008, **319**, 939–943.
117 J. An and N. L. Rosi, *J. Am. Chem. Soc.*, 2010, **132**, 5578–5579.
118 O. J. García-Ricard and A. J. Hernández-Maldonado, *J. Phys. Chem. C*, 2010, **114**, 1827–1834.
119 K. L. Mulfort, O. K. Farha, C. D. Malliakas, M. G. Kanatzidis and J. T. Hupp, *Chem.–Eur. J.*, 2010, **16**, 276–281.
120 R. Kitaura, R. Matsuda, Y. Kubota, S. Kitagawa, M. Takata, T. C. Kobayashi and M. Suzuki, *J. Phys. Chem. B*, 2005, **109**, 23378–23385.
121 Y.-S. Bae, B. G. Hauser, O. K. Farha, J. T. Hupp and R. Q. Snurr, *Microporous Mesoporous Mater.*, 2011, **141**, 231–235.
122 J. Lincke, D. Lässig, J. Moellmer, C. Reichenbach, A. Puls, A. Moeller, R. Gläser, G. Kalies, R. Staudt and H. Krautscheid, *Microporous Mesoporous Mater.*, 2011, **142**, 62–69.
123 J. A. Tian, R. K. Motkuri, P. K. Thallapally and B. P. McGrail, *Cryst. Growth Des.*, 2010, **10**, 5327–5333.
124 Y.-S. Bae, D. Dubbeldam, A. Nelson, K. S. Walton, J. T. Hupp and R. Q. Snurr, *Chem. Mater.*, 2009, **21**, 4768–4777.
125 P. Pachfule, R. Das, P. Poddar and R. Banerjee, *Cryst. Growth Des.*, 2011, **11**, 1215–1222.
126 J. Zhang, H. Wu, T. J. Emge and J. Li, *Chem. Commun.*, 2010, **46**, 9152–9154.
127 F. Thétiot, C. Duhayon, T. S. Venkatakrishnan and J.-P. Sutter, *Cryst. Growth Des.*, 2008, **8**, 1870–1877.
128 P. K. Thallapally, J. Tian, M. R. Kishan, C. A. Fernandez, S. J. Dalgarno, P. B. McGrail, J. E. Warren and J. L. Atwood, *J. Am. Chem. Soc.*, 2008, **130**, 16842–16843.
129 M. R. Kishan, J. Tian, P. K. Thallapally, C. A. Fernandez, S. J. Dalgarno, J. E. Warren, B. P. McGrail and J. L. Atwood, *Chem. Commun.*, 2010, **46**, 538–540.
130 P. Pachfule, R. Das, P. Poddar and R. Banerjee, *Cryst. Growth Des.*, 2010, **10**, 2475–2478.
131 H. J. Park, Y. E. Cheon and M. P. Suh, *Chem.–Eur. J.*, 2010, **16**, 11662–11669.
132 S.-S. Chen, M. Chen, S. Takamizawa, M.-S. Chen, Z. Su and W.-Y. Sun, *Chem. Commun.*, 2011, **47**, 752–754.
133 H. Wu, R. S. Reali, D. A. Smith, M. C. Trachtenberg and J. Li, *Chem.–Eur. J.*, 2010, **16**, 13951–13954.
134 C. A. Fernandez, P. K. Thallapally, R. K. Motkuri, S. K. Nune, J. C. Sumrak, J. Tian and J. Liu, *Cryst. Growth Des.*, 2010, **10**, 1037–1039.
135 P. Chowdhury, C. Bikkina and S. Gumma, *J. Phys. Chem. C*, 2009, **113**, 6616–6621.
136 O. K. Farha, A. M. Spokoyny, K. L. Mulfort, M. F. Hawthorne, C. A. Mirkin and J. T. Hupp, *J. Am. Chem. Soc.*, 2007, **129**, 12680–12681.
137 Y.-S. Bae, O. K. Farha, A. M. Spokoyny, C. A. Mirkin, J. T. Hupp and R. Q. Snurr, *Chem. Commun.*, 2008, 4135–4137.
138 B. Wang, A. P. Côte, H. Furukawa, M. O'Keeffe and O. M. Yaghi, *Nature*, 2008, **453**, 207–212.
139 J.-P. Zhang and X.-M. Chen, *J. Am. Chem. Soc.*, 2009, **131**, 5516–5521.
140 P. Pachfule, T. Panda, C. Dey and R. Banerjee, *CrystEngComm*, 2010, **12**, 2381–2389.
141 S. R. Miller, P. A. Wright, T. Devic, C. Serre, G. Férey, P. L. Llewellyn, R. Denoyel, L. Gaberova and Y. Filinchuk, *Langmuir*, 2009, **25**, 3618–3626.
142 Y.-J. Zhang, T. Liu, S. Kanegawa and O. Sato, *J. Am. Chem. Soc.*, 2010, **132**, 912–913.
143 A. Mallick, S. Saha, P. Pachfule, S. Roy and R. Banerjee, *J. Mater. Chem.*, 2010, **20**, 9073–9080.
144 Z. Bao, S. Alnemrat, L. Yu, I. Vasiliev, Q. Ren, X. Lu and S. J. Deng, *J. Colloid Interface Sci.*, 2011, **357**, 504–509.
145 J. D. Figueroa, T. Fout, S. Plasynski, H. McIlvried and R. D. Srivastava, *Int. J. Greenhouse Gas Control*, 2008, **2**, 9–20.
146 F. Gándara, E. Gutiérrez-Puebla, M. Iglesias, N. Snejko and M. A. Monge, *Cryst. Growth Des.*, 2010, **10**, 128–134.
147 J. T. Culp, A. L. Goodman, D. Chirdon, S. G. Sankar and C. Matranga, *J. Phys. Chem. C*, 2010, **114**, 2184–2191.
148 J. B. Lambert, Z. Liu and C. Liu, *Organometallics*, 2008, **27**, 1464–1469.
149 M. Xue, Y. Liu, R. M. Schaffino, S. Xiang, X. Zhao, G.-S. Zhu, S.-L. Qui and B. Chen, *Inorg. Chem.*, 2009, **48**, 4649–4651.
150 B.-Q. Ma, K. L. Mulfort and J. T. Hupp, *Inorg. Chem.*, 2005, **44**, 4912–4914.

151 N. L. Rosi, J. Kim, M. Eddaoudi, B. Chen, M. Ó'Keeffe and O. M. Yaghi, *J. Am. Chem. Soc.*, 2005, **127**, 1504–1518.
152 Q. M. Wang, D. Shen, M. Bulow, M. L. Lau, S. Deng, F. R. Fitch, N. O. Lemcoff and J. Semanscin, *Microporous Mesoporous Mater.*, 2002, **55**, 217–230.
153 P. L. Llewellyn, S. Bourrelly, C. Serre, A. Vimont, M. Daturi, L. Hamon, G. Weireld, J.-S. Chang, D.-Y. Hong, Y. K. Hwang, S. H. Jhung and G. Férey, *Langmuir*, 2008, **24**, 7245–7250.
154 P. D. C. Dietzel, V. Besikiotis and R. Blom, *J. Mater. Chem.*, 2009, **19**, 7362–7370.
155 Y. E. Cheon and M. P. Suh, *Chem. Commun.*, 2009, 2296–2298.
156 Y. E. Cheon and M. P. Suh, *Chem.–Eur. J.*, 2008, **14**, 3961–3967.
157 Y. E. Cheon, J. Park and M. P. Suh, *Chem. Commun.*, 2009, 5436–5438.
158 S. Bourrelly, P. L. Llewellyn, C. Serre, F. Millange, L. Loiseau and G. Férey, *J. Am. Chem. Soc.*, 2005, **127**, 13519–13521.
159 P. L. Llewellyn, S. Bourrelly, C. Serre, Y. Filinchuk and G. Ferey, *Angew. Chem.*, 2006, **118**, 7915–7918.
160 S. Galli, N. Masciocchi, G. Tagliabue, A. Sironi, J. A. R. Navarro, J. M. Salas, L. Mendez-Linan, M. Domingo, M. Perez and E. Barea, *Chem.–Eur. J.*, 2008, **14**, 9890–9891.
161 Y.-S. Bae, O. K. Farha, J. T. Hupp and R. Q. Snurr, *J. Mater. Chem.*, 2009, **19**, 2131–2134.
162 S. Couck, J. F. M. Denayer, G. V. Baron, T. Rémy, J. Gascon and F. Kapteijn, *J. Am. Chem. Soc.*, 2009, **131**, 6326–6327.
163 D. W. Keith, H. D. Minh and J. K. Stolaroff, *Clim. Change*, 2006, **74**, 17–45.
164 K. S. Walton and M. D. LeVan, *Sep. Sci. Technol.*, 2006, **41**, 485–500.
165 P. J. E. Harlick and F. H. Tezel, *Microporous Mesoporous Mater.*, 2004, **76**, 71–79.
166 S. Xiang, Y. He, Z. Zhang, H. Wu, W. Zhou, R. Krishna and B. Chen, *Nat. Commun.*, 2012, **495**, 80–84.
167 S. Cavenati, C. A. Grande and A. E. Rodrigues, *Ind. Eng. Chem. Res.*, 2008, **47**, 6333–6335.
168 M. Schubert, U. Müller, M. Hesse and U. Diehlmann, *Process for Preparing Porous Metal-Organic Framework Materials*, WO/2007/090809, 2007.
169 J. Lee, Synthesis and Gas Sorption Study of Microporous Metal Organic Frameworks for Hydrogen and Methane Storage, UMI, 3319649, 7, 2007.
170 S. S. Kaye, A. Dailly, O. M. Yaghi and J. R. Long, *J. Am. Chem. Soc.*, 2007, **129**, 14176–14177.
171 J. J. Low, A. I. Benin, P. Jakubczak, J. F. Abrahamian, S. A. Faheem and R. R. Willis, *J. Am. Chem. Soc.*, 2009, **131**, 15834–15842.
172 S. L. James, *Chem. Soc. Rev.*, 2003, **32**, 276–288.
173 L. Valenzano, B. Civellari, K. Sillar and J. Sauer, *J. Phys. Chem. C*, 2011, **115**, 21777–21784.
174 L. MacGillivray, *Metal-Organic Frameworks: Design and Application*, John Wiley & Sons, Inc., Hoboken, New jersey, 2010.
175 R. C. Wade and M. Dinca, *Dalton Trans.*, 2012, **41**, 7931–7938.
176 A. L. Dzubak, L.-C. Lin, J. Kim, J. A. Swisher, R. Poloni, S. N. Maximoff, B. Smit and L. Gagliardi, *Nat. Chem.*, 2012, **4**, 810–816.
177 A. Kondo, A. Chinen, H. Kajiro, T. Nakagawa, K. Kato, M. Takata, Y. Hattori, F. Okino, T. Ohba, K. Kaneko and H. Kanoh, *Chem.–Eur. J.*, 2009, **15**, 7549–7553.
178 A. Y. Robin and K. M. Fromm, *Coord. Chem. Rev.*, 2006, **250**, 2127–2157.
179 L. Ciemnolonski, *Ligand Engineering for Metal-Organic Frameworks with Hydrogen Storage Capabilities*, Drexel University, Dept. of Chemistry, Philadelphia, PA, December 5, 2009.
180 R. Babarao and J. Jiang, *Langmuir*, 2008, **24**, 6270–6278.
181 A. Torrisi, C. Mellot-Draznieks and R. G. Bell, *J. Chem. Phys.*, 2009, **130**, 194703.
182 A. Torrisi, C. Mellot-Draznieks and R. G. Bell, *J. Chem. Phys.*, 2010, **132**, 044705.
183 H. Deng, S. Grunder, K. E. Cordova, C. Valente and O. M. Yaghi, *Science*, 2012, **336**, 1018–1023.
184 J. W. Yoon, S. H. Jhung, Y. K. Hwang, S. M. Humphrey, P. T. Wood and J. S. Chang, *Adv. Mater.*, 2007, **19**, 1830–1834.
185 D. G. Samsonenko, H. Kim, Y. Y. Sun, G. H. Kim, H. S. Lee and K. Kim, *Chem.–Asian J.*, 2007, **2**, 484–488.
186 Y.-S. Bae, A. M. Spokoyny, O. K. Farha, R. Q. Snurr, J. T. Hupp and C. A. Mirkin, *Chem. Commun.*, 2010, **46**, 3478–3480.
187 M. Radosz, X. Hu, K. Krutkramelis and Y. Shen, *Ind. Eng. Chem. Res.*, 2008, **47**, 3783–3794.
188 Q. Xu, D. H. Liu, Q. Y. Yang, C. L. Zhong and J. G. Mi, *J. Mater. Chem.*, 2010, **20**, 706–714.
189 S. Bordiga, L. Regli, F. Bonino, E. Groppo, C. Lamberti, B. Xiao, P. S. Wheatley, R. E. Morris and A. Zecchina, *Phys. Chem. Chem. Phys.*, 2007, **9**, 2676–2685.
190 J. L. Anthony, S. N. V. K. Aki, E. J. Maginn and J. F. Brennecke, *Int. J. Environ. Technol. Manage.*, 2004, **4**, 105–115.
191 C. Cadena, J. L. Anthony, J. K. Shah, T. I. Morrow, J. F. Brennecke and E. J. Maginn, *J. Am. Chem. Soc.*, 2004, **126**, 5300–5308.
192 A. U. Czaja, N. Trukhan and U. Muller, *Chem. Soc. Rev.*, 2009, **38**, 1284–1293.
193 R. Banerjee, A. Phan, B. Wang, C. Knobler, H. Furukawa, M. O'Keeffe and O. M. Yaghi, *Science*, 2008, **319**, 939–943.
194 S. Keskin, T. M. Van Heest and D. S. Sholl, *ChemSusChem*, 2010, **3**, 879–891.
195 S. Keskin, J. Liu, R. B. Rankin, J. K. Johnson and D. S. Sholl, *Ind. Eng. Chem. Res.*, 2009, **48**, 2355–2371.
196 E. F. da Silva and H. F. Svendsen, *Int. J. Greenhouse Gas Control*, 2007, **1**, 151–157.
197 H. Wu, J. M. Simmons, G. Srinivas, W. Zhou and T. Yildirim, *J. Phys. Chem. Lett.*, 2010, **1**, 1946–1951.
198 Q. Y. Yang and C. L. Zhong, *J. Phys. Chem. B*, 2006, **110**, 17776–17783.
199 R. Babarao, J. W. Jiang and S. I. Sandler, *Langmuir*, 2009, **25**, 5239–5247.

200 J. Lan, D. Cao, W. Wang and B. Smit, *ACS Nano*, 2010, **4**, 4225–4237.
201 T. Loiseau, L. Lecroq, C. Volkringer, J. Marrot, G. Frey, M. Haouas, F. Taulelle, S. Bourrelly, P. L. Llewellyn and M. Latroche, *J. Am. Chem. Soc.*, 2006, **128**, 10223–10230.
202 T. Düren and R. Q. Snurr, *J. Phys. Chem. B*, 2004, **108**, 15703–15708.
203 A. Martín-Calvo, E. Garcia-Perez, J. M. Castillo and S. Calero, *J. Phys. Chem.*, 2008, **10**, 7085–7091.
204 J. A. Greathouse, T. L. Kinnibrugh and M. D. Allendorf, *Ind. Eng. Chem. Res.*, 2009, **48**, 3425–3431.
205 Q. Yang, Q. Xu, B. Liu, C. Zhong and B. Smit, *Chin. J. Chem. Eng.*, 2009, **17**, 781–790.
206 R. Babarao, Y. H. Tong and J. Jiang, *J. Phys. Chem. B*, 2009, **113**, 9129–9136.
207 M. Gallo and D. Glossman-Mitnik, *J. Phys. Chem. C*, 2009, **113**, 6634–6642.
208 T. Fukushima, S. Horike, Y. Inubushi, K. Nakagawa, Y. Kubota, M. Takata and S. Kitagawa, *Angew. Chem., Int. Ed.*, 2010, **49**, 4820–4824.
209 S. R. Batten, S. M. Neville and D. R. Turner, *Coordination Polymers: Design, Analysis and Application*, Royal Society of Chemistry, Cambridge, 2009.
210 S. Q. Ma, J. Eckert, P. M. Forster, J. W. Yoon, Y. K. Hwang, J. S. Chang, C. D. Collier, J. B. Parise and H. C. Zhou, *J. Am. Chem. Soc.*, 2008, **130**, 15896–15902.
211 B. Chen, N. W. Ockwing, A. R. Millward, D. S. Contreras and O. M. Yaghi, *Angew. Chem., Int. Ed.*, 2005, **44**, 4745–4749.
212 M. Dinca, A. Dailly, Y. Liu, C. M. Brown, D. A. Neumann and J. R. Long, *J. Am. Chem. Soc.*, 2006, **128**, 16876–16883.
213 B. Xiao, P. S. Wheatley, X. B. Zhao, A. J. Fletcher, S. Fox, A. G. Rossi, I. L. Megson, S. Bordiga, L. Regli, K. M. Thomas and R. E. Morris, *J. Am. Chem. Soc.*, 2007, **129**, 1203–1209.
214 A. O. Yazaydin, R. Q. Snurr, T.-H. Park, K. Koh, J. Liu, M. D. LeVan, A. I. Benin and P. Jaku, *Science*, 2004, **305**, 352.
215 S. S.-Y. Chui, S. M.-F. Lo, J. P. H. Charmant, A. G. Orpen and I. D. Williams, *Science*, 1999, **283**, 1148–1150.
216 S. S. Kaye, A. Dailly, O. M. Yaghi and J. R. Long, *J. Am. Chem. Soc.*, 2007, **129**, 14176–14177.
217 A. N. Dickey, A. Yazaydin, R. R. Willis and R. Q. Snurr, *Can. J. Chem. Eng.*, 2012, **90**, 825–832.
218 E. Stavitski, E. A. Pidko, S. Couck, T. Remy, E. J. M. Hensen, B. M. Weckhuysen, J. Denayer, J. Gascon and F. Kapteijn, *Langmuir*, 2011, **27**, 3970–3976.
219 (*a*) N. Planas, A. L. Dzubak, R. Poloni, L.-C. Lin, A. McManus, T. M. McDonald, J. B. Neaton, J. R. Long, B. Smit and L. Gagliardi, *J. Am. Chem. Soc.*, 2013, **135**, 7402–7405; (*b*) O. K. Farha, K. L. Mulfort and J. T. Hupp, *Inorg. Chem.*, 2008, **47**, 10223–10225.
220 Z. Wang and S. M. Cohen, *J. Am. Chem. Soc.*, 2007, **129**, 12368–12369.
221 Z. Wang and S. M. Cohen, *J. Am. Chem. Soc.*, 2009, **131**, 16675–16677.
222 M. Savonnet, D. Baser-Bachi, N. Bats, J. Perez-Pellitero, E. Jeanneau, V. Lecocq, C. Pine and D. Farrusseng, *J. Am. Chem. Soc.*, 2010, **132**, 4518–4519.
223 (*a*) S. J. Garibay and S. M. Cohen, *Chem. Commun.*, 2010, **46**, 7700–7702; (*b*) K. Leus, S. Couck, M. Vandichel, G. Vanhaelewyn, Y.-Y. Liu, G. B. Marin, I. V. Driessche, D. Depla, M. Waroquier, V. V. Speybroeck, J. F. M. Denayerb and P. Van Der Voort, *Phys. Chem. Chem. Phys.*, 2012, **14**, 15562–15570.
224 S. Bernt, V. Guillerm, C. Serre and N. Stock, *Chem. Commun.*, 2011, **47**, 2838–2840.
225 W. Mu, D. Liu and C. Zhong, *Microporous Mesoporous Mater.*, 2011, **143**, 66–72.
226 P. Dalach, H. Frost, R. Q. Snurr and D. E. Ellis, *J. Phys. Chem. C*, 2008, **112**, 9278.
227 E. Klontzas, A. Mavrandonakis, E. Tylianakis and G. E. Froudakis, *Nano Lett.*, 2008, **8**, 1572–1576.
228 K. L. Mulfort, O. K. Farha, C. L. Stern, A. A. Sarjeant and J. T. Hupp, *J. Am. Chem. Soc.*, 2009, **131**, 3866–3868.
229 D. Himsl, D. Wallacher and M. Hartmann, *Angew. Chem., Int. Ed.*, 2009, **121**, 4710–4714.
230 O. K. Farha, Y.-S. Bae, B. G. Hauser, A. M. Spokoyny, R. Q. Snurr, C. A. Mirkin and J. T. Hupp, *Chem. Commun.*, 2010, **46**, 1056–1058.
231 J. W. Jiang, Metal–organic frameworks for CO2 capture: what are learned from molecular simulations, *Coordination Polymers and Metal Organic Frameworks*, Nova Science Publishers, 2012, pp. 225–247.
232 C. A. Fernandez, P. K. Thallapally, R. K. Motkuri, S. K. Nune, J. C. Sumrak and J. Tian, *Cryst. Growth Des.*, 2010, **10**, 1037–1039.
233 L. Hamon, C. Serre, T. Devic, T. Loiseau, F. Millange, G. Ferey and G. De Weireld, *J. Am. Chem. Soc.*, 2009, **131**, 8775–8777.
234 L. Hamon, A. Vimont, C. Serre, T. Devic, A. Ghoufi, G. Maurin, T. Loiseau, F. Millange, M. Daturi, G. Ferey, G. De Weireld, *Characterization of Porous Solids VIII - Proceedings of the 8th International Symposium of the Characterization of Porous Solids*, Royal Society of Chemistry, 2009, vol. 318, p. 25.
235 L. Huang, H. Wang, J. Chen, Z. Wang, J. Sun, D. Zhao and Y. Yan, *Microporous Mesoporous Mater.*, 2003, **58**, 105–114.
236 J. A. Greathouse and M. D. Allendorf, *J. Am. Chem. Soc.*, 2006, **128**, 10678–10679.
237 H. J. Choi, M. Dincâ, A. Dailly and J. R. Long, *Energy Environ. Sci.*, 2010, **3**, 117–123.
238 S. Galli, N. Masciocchi, V. Colombo, A. Maspero, G. Palmisiano, E. Barea, F. J. López-Garzón, M. Domingo-Garciá, I. Fernández-Morales and J. A. R. Navarro, *Chem. Mater.*, 2010, **22**, 1664–1972.
239 V. Colombo, S. Galli, H.-J. Choi, G. D. Han, A. Maspero, G. Palmisiano, N. Masciocchi and J. R. Long, *Chem. Sci.*, 2011, **2**, 1311–1319.
240 S. Horike, S. Shimomura and S. Kitagawa, Soft porous crystals, *Nat. Chem.*, 2009, **1**, 695–704.
241 C.-D. Wu and W. Lin, *Angew. Chem., Int. Ed.*, 2007, **46**, 1075–1078.
242 C. Petit and T. J. Bandosz, *Dalton Trans.*, 2012, **41**, 4027–4035.
243 W. J. Work, K. Horie, M. Hes and R. F. T. Stepto, *Pure Appl. Chem.*, 2004, **76**, 1985–2007.

